2011

Modeling gross primary production of irrigated and rain-fed maize using MODIS imagery and CO_2 flux tower data

Joshua L. Kalfas
University of Oklahoma, joshua.l.kalfas@ou.edu

Xiangming Xiao
University of Oklahoma, xiangming.xiao@ou.edu

Diana X. Vanegas
University of Oklahoma, dianaxime@ou.edu

Shashi B. Verma
University of Nebraska-Lincoln, sverma1@unl.edu

Andrew E. Suyker
University of Nebraska-Lincoln, asuyker1@unl.edu

Follow this and additional works at: http://digitalcommons.unl.edu/natrespapers

Part of the Agriculture Commons, Agronomy and Crop Sciences Commons, Environmental Monitoring Commons, Natural Resources and Conservation Commons, Natural Resources Management and Policy Commons, Other Earth Sciences Commons, and the Other Environmental Sciences Commons

Modeling gross primary production of irrigated and rain-fed maize using MODIS imagery and CO$_2$ flux tower data

Joshua L. Kalfas,[1] Xiangming Xiao,[1] Diana X. Vanegas,[1] Shashi B. Verma,[2] and Andrew E. Suyker[2]

1 Department of Botany and Microbiology, Center for Spatial Analysis, University of Oklahoma, 101 David L. Boren Blvd., Norman, OK 73019
2 School of Natural Resources, University of Nebraska–Lincoln, Lincoln NE 68583

Corresponding author — X. Xiao, tel 405-325-8941, email xiangming.xiao@ou.edu

Abstract

Information on gross primary production (GPP) of maize croplands is needed for assessing and monitoring maize crop conditions and the carbon cycle. A number of studies have used the eddy covariance technique to measure net ecosystem exchange (NEE) of CO$_2$ between maize cropland fields and the atmosphere and partitioned NEE data to estimate seasonal dynamics and interannual variation of GPP in maize fields having various crop rotation systems and different water management practices. How to scale up in situ observations from flux tower sites to regional and global scales is a challenging task. In this study, the Vegetation Photosynthesis Model (VPM) and satellite images from the Moderate Resolution Imaging Spectroradiometer (MODIS) are used to estimate seasonal dynamics and interannual variation of GPP during 2001–2005 at five maize cropland sites located in Nebraska and Minnesota of the U.S.A. These sites have different crop rotation systems (continuously maize vs. maize and soybean rotated annually) and different water management practices (irrigation vs. rainfed). The VPM is based on the concept of light absorption by chlorophyll and is driven by the Enhanced Vegetation Index (EVI) and the Land Surface Water Index (LSWI), photosynthetically active radiation (PAR), and air temperature. The seasonal dynamics of GPP predicted by the VPM agreed well with GPP estimates from eddy covariance flux tower data over the period of 2001–2005. These simulation results clearly demonstrate the potential of the VPM to scale-up GPP estimation of maize cropland, which is relevant to food, biofuel, and feedstock production, as well as food and energy security.

Keywords: Production efficiency model, Vegetation Photosynthesis Model (VPM), Carbon fluxes, C4 photosynthesis, Corn

1. Introduction

Accurate and updated information on gross primary production (GPP) of croplands is of vital importance, with variations in productivity impacting global food security, the global carbon cycle, and the global water cycle, but physical characteristics of cropland fields, biological characteristics of crops, and climatic characteristics of a region all affect cropland productivity. The spatial and temporal distributions of these characteristics vary substantially since each characteristic is the resultant combination of numerous underlying factors. Cropland productivity can vary significantly, even within a small field of homogeneous crop (Ping and Dobermann, 2005; Ping et al., 2008).

The extent of spatial and temporal variability affecting cropland productivity can be seen in maize production. A common agricultural practice within the United States of America (U.S.A.) is the annual rotation of maize and soybean in a crop field. In 2008, 35.3 million hectares of maize and 30.1 million hectares of soybean were planted across the U.S.A. (NASS, 2008). These areas are comparable to a continuously maize field slightly smaller than Germany and a continuously soybean field approximately equal in area to Italy. The U.S.A. is the largest maize producer and the largest exporter of maize grains in the world, accounting for approximately 50% of global exports (http://www.ers.usda.gov/Briefing/Corn/) valued at US$ 11.9 billion for 2008 (http://www.ers.usda.gov/Data/FATUS/).

Numerous studies have examined maize cropland productivity for various reasons. One of these reasons is to understand the net ecosystem exchange (NEE) of carbon dioxide (CO$_2$) between cropland fields and the atmosphere, since NEE is used to assess carbon sequestration capacities of croplands. NEE is defined as the difference between GPP and ecosystem respiration (R_e). GPP has been used to quantify crop productivity, assist in identifying best management practices (Baker and Griffis, 2005; Baker et al., 2007), and understand temporal variations in productivity (Falge et al., 2002a, 2002b). Both GPP and NEE fluxes from croplands and other terrestrial ecosystems are important for monitoring atmospheric CO$_2$ flux (Baldocchi et al., 2001; Falge et al., 2002a, 2002b).

Concerns of climate change impacts and development of possible mitigation strategies require understanding the magnitude and timing of CO_2 fluxes from both managed and natural ecosystems.

CO_2 eddy covariance flux towers (hereafter, flux towers) deployed in agricultural fields having different site characteristics have proven helpful in understanding flux variability. When NEE of irrigated and rain-fed maize cropland was quantified and contrasted, night time NEE showed strong soil temperature dependence, although it was significantly smaller at the rain-fed site during moisture stress periods (Suyker et al., 2004). In a study that quantified GPP and R_e of maize croplands in terms of controlling variables such as air temperature, relative humidity, and soil temperature (Suyker et al., 2005), the results showed that seasonal changes in green leaf area index explained about 95% of seasonal variability in GPP. Another study (Verma et al., 2005) compared seasonal and annual exchanges of CO_2 from maize and soybean croplands, evaluated the impacts of irrigation on CO_2 exchange, and assessed the impacts of crop rotation on CO_2 exchange. The results showed that maize–soybean rotation systems varied from being carbon neutral to slight carbon sources. However, the carbon budget of no-till maize–soybean rotation systems has also been reported to be a small net carbon sink (Hollinger et al., 2005, 2006a, 2006b; Dobermann et al., 2006). Although data obtained from flux towers have greatly increased our understanding of cropland carbon-flux dynamics, the expense and maintenance of flux towers in addition to the inaccessibility of certain sites limits their effectiveness for extensive observations. Further, the aforementioned spatial and temporal variability of croplands restricts the use of study results to sites with similar characteristics. There is a need to scale up observations beyond the spatial limits of flux tower footprints and sites similar to those studied.

Satellite remote sensing provides an avenue to scale up observations from flux towers to greater regions. Remotely sensed data is usually spatially continuous and observed at regular intervals. Images from passive optical sensors have long been used for characterizing spatial variability in agricultural fields (Bhatti et al., 1991). These observations are used in numerous physical models and are becoming increasingly used in biophysical modeling; a number of techniques for assimilating remote sensing data into agro-ecosystem models were recently reviewed (Dorigo et al., 2007). Several satellite-based light-use efficiency (LUE) models have been used to estimate gross and net primary production of natural vegetation and croplands (Choudhury, 2001; Running et al., 2004; Bradford et al., 2005; Sims et al., 2006, 2008; Yuan et al., 2007). The Vegetation Photosynthesis Model (VPM), which is driven by two vegetation indices and climate data (Xiao et al., 2004a), belongs to the LUE model family. The VPM has previously been described in detail (Xiao et al., 2004a, 2005b) and evaluated in alpine grassland (Li et al., 2007), temperate grassland (Wu et al., 2008), evergreen needle-leaf forest (Xiao et al., 2004a, 2005b), old-growth temperate mixed forest (Wu et al., 2009), temperate deciduous broadleaf forest (Xiao et al., 2004b), seasonally moist tropical evergreen forest (Xiao et al., 2005c), maize cropland and degraded grassland (Wang et al., 2010b), and winter wheat and maize double-cropped agricultural systems in China (Yan et al., 2009). Seasonal dynamics of VPM-predicted GPP agreed well with GPP estimated from flux tower observations in the above-mentioned case studies (a correlation coefficient of 0.9 or higher).

The objectives of this study are (1) to characterize the biophysical performance of vegetation indices for identifying maize crop phenology, and (2) to evaluate the performance of the VPM in estimating seasonal dynamics of GPP for maize cropland sites, where crop rotation (continuously maize vs. maize and soybean rotated annually) and water management (irrigation vs. rain-fed) differ.

2. The study sites, data, and methods

2.1. A brief description of the study sites

Climate and CO_2 data were obtained from five flux towers maintained within maize croplands. These croplands are cultivated as either continuously maize or as an annual rotation of maize and soybean (Table 1). A common practice of maize cultivation is to plant after the average air temperature exceeds 10 °C. Maize seeds typically geminate and emerge from the soil within 5–30 days of planting, depending upon soil temperature and moisture. At the end of the season, farmers often leave maize crops drying in the field for several days before harvest. Due to these practices, three distinct periods are differentiated in this study for clarity: (1) the plant growing season, which is the entire portion of a year where native vegetation may actively grow and crop cultivation is possible; (2) the cultivation period, beginning at planting and ending at harvest; and (3) the crop-growth period, beginning at crop emergence and ending at crop senescence. How site characteristics and cultivation practices vary between the maize fields is shown in Table 2. Unless otherwise noted, all site information discussed in this paper was obtained from the Site Information pages of the AmeriFlux website (http://public.ornl.gov/ameriflux/).

2.1.1. The Mead sites (Mead, Nebraska)

Three flux tower sites, Mead Irrigated, Mead Irrigated Rotation, and Mead Rainfed, are located at the University of Nebraska Agricultural Research and Development Center, near Mead, Nebraska, U.S.A. These three sites, all within 1.6 km of one another, have deep, silty clay-loam soils, a temperate continental climate, and are at the western edge of the favorably rain-fed 'Corn Belt'. Here, the growing season usually begins in May and ends in October. The primary differences between these three sites are crop rotation and water management. The Mead Irrigated site is a continuously maize cropland receiving additional water when necessary via a center-pivot irrigation system. The Mead Irrigated Rotation site is similar to the Mead Irrigated site but annually rotates between maize and soybean cultivation. The Mead Rainfed site also annually rotates between maize and soybean cultivation, but it completely relies on rainfall for crop water requirements.

The three Mead sites have highly similar seasonal dynamics of PAR, temperature, and precipitation (Figure 1). Approximately 55% of annual precipitation occurs during the cultivation period at these three sites, while a large portion of the other 45% occurs during late winter and early spring. Irrigation at the Mead Irrigated and Mead Irrigated Rotation sites approximately doubles the amount of water available when compared

Table 1. The geographic locations and crops cultivated at the five flux tower sites in Nebraska and Minnesota, U.S.A.

Site name	Latitude (°)	Longitude (°)	Elevation (m)	2001	2002	2003	2004	2005
Mead Irrigated	41.1651	−96.4766	361	Maize	Maize	Maize	Maize	Maize
Mead Irrigated Rotation	41.1649	−96.4701	362	Maize	Soybean	Maize	Soybean	Maize
Mead Rainfed	41.1797	−96.4396	362	Maize	Soybean	Maize	Soybean	Maize
Rosemount G19	44.7217	−93.0893	260				Soybean	Maize
Rosemount G21	44.7143	−93.0898	260				Soybean	Maize

Table 2. Site characteristics of the five study sites in Nebraska and Minnesota, U.S.A. Field areas are approximate.

Site name	Field area (m²)	Irrigation type	Canopy height (m)	EC measurement height(s) (m)	Minimum fetch (m)	Other fetches (m)		
Mead Irrigated	~487,000	Center-pivot	2.9	3 (canopy <1 m)	500[a]	–	–	–
				6 (until harvest)				
Mead Irrigated Rotation	~524,000	Center-pivot	2.9	3 (canopy <1 m)	500[a]	–	–	–
				6 (until harvest)				
Mead Rainfed	~645,000	none	2.9	3 (canopy <1 m)	500[a]	–	–	–
				6 (until harvest)				
Rosemount G19	~376,357	none	2.8	2–4 (variable)	196 (north)	412 (south)	317 (east)	388 (west)
Rosemount G21	~182,109	none	2.8	2–4 (variable)	182 (east)	186 (south)	188 (north)	261 (west)

a. The minimum fetch of 500 m is similar in all directions for the two center-pivot irrigation sites. For the Mead Rainfed site, the minimum fetch is approximated from the center-pivot arm of the two irrigated fields, although the fetches for this site are larger than the two irrigated fields.

to precipitation alone (precipitation in Figure 1 includes irrigation). In comparison to the irrigated sites, approximately 25% and 35% less crop seeds was sown per area in the Mead Rainfed field to account for differences in water-limited attainable yield in 2001 and 2003, respectively (Verma et al., 2005); this practice continued in 2005.

2.1.2. The Rosemount sites (St. Paul, Minnesota)

Two flux tower sites, Rosemount G19 and Rosemount G21, are located at the University of Minnesota's Rosemount Research and Outreach Center, approximately 25 km south of St. Paul,

Minnesota, U.S.A. (Baker and Griffis, 2005). These two adjacent sites are separated by a road and have a silty loam soil with a surface layer of high organic carbon content. Both sites have a temperate continental climate and a regional growing season that usually begins in May and ends in October.

Due to their spatial proximity, the two Rosemount sites have highly similar seasonal dynamics of PAR, temperature, and precipitation (Figure 2). Both of these sites depend on precipitation during cultivation. No irrigation occurs. Approximately 63% of the annual precipitation occurred during the cultivation-period at these rain-fed sites.
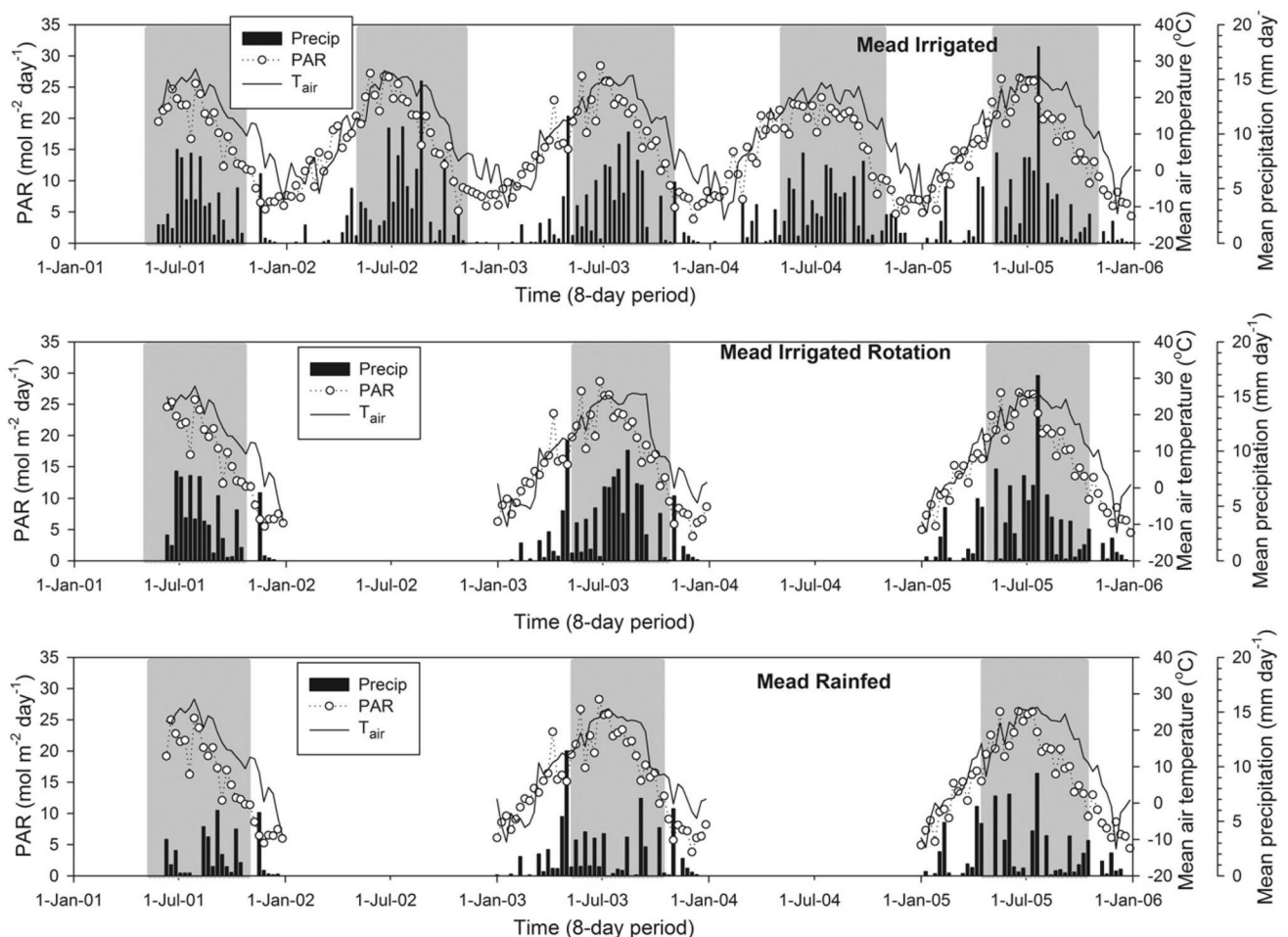

Figure 1. Seasonal and interannual variation of precipitation (Precip), photosynthetically active radiation (PAR), and air temperature (T_{air}) observed at the three flux tower sites in Mead, Nebraska, U.S.A. during 2001–2005, with the cultivation periods highlighted: (a) the irrigated, continuously maize site, (b) the irrigated, annual maize–soybean rotation site, and (c) the rain-fed, annual maize–soybean rotation site.
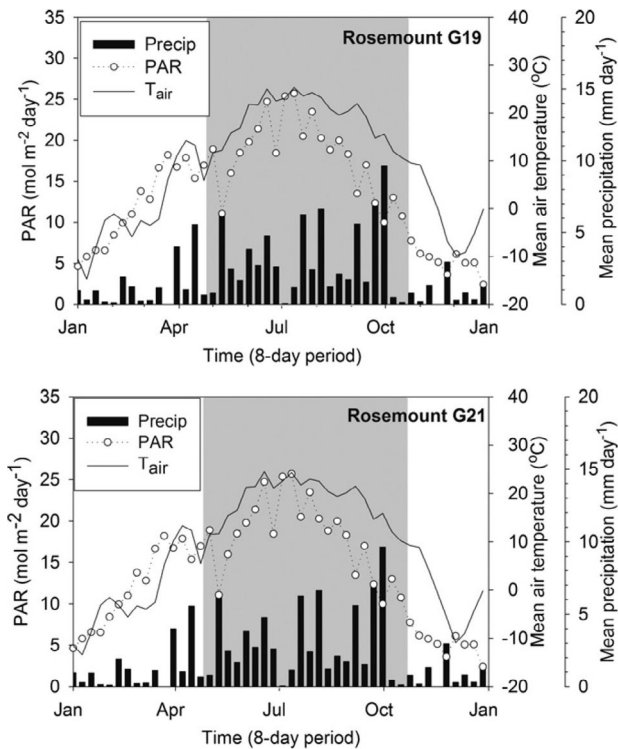
Figure 2. Seasonal and interannual variation of precipitation (Precip), photosynthetically active radiation (PAR), and air temperature (T_{air}) observed at the two flux tower sites in Rosemount, Minnesota, U.S.A. during 2005, with the cultivation periods highlighted: (a) the Rosemount G19 site and (b) the Rosemount G21 site.

2.2. Site-specific climate data and CO_2 flux data

All flux tower data used in this study were downloaded from Ameriflux (http://public.ornl.gov/ameriflux/), part of a global network of micrometeorological towers known as FLUXNET (http://daac.ornl.gov/FLUXNET/; (Baldocchi et al., 2001)). The Ameriflux network provides continuous observations of CO_2, water, and energy fluxes at the ecosystem and landscape levels. It also provides standard datasets of climate and CO_2 fluxes to the public, after various levels of data processing have been completed. Eight-day period, Level 4 data were used in this study; therefore, flux tower and MODIS observation periods are consistent for comparison. In this study, original marginal distribution sampling (MDS) gap-filled data (Reichstein et al., 2005) were used for analysis for two reasons: (1) the site investigators were determined to be the most knowledgeable and competent individuals for identifying and correcting poor-quality data; and (2) these datasets are available for each site as opposed to standard MDS gap-filled data which are absent in various datasets. The average data coverage for this network of flux towers during years is 65%, 69% and 75% for NEE, latent heat, and sensible heat, respectively, due to system failures or data rejection; therefore, robust and consistent gap-filling methods are required to provide complete data sets (Falge et al., 2001a and Falge et al., 2001b). In these datasets, negative NEE values denote carbon uptake, and positive NEE values denote carbon release.

2.3. MODIS imagery and vegetation indices

The Moderate Resolution Imaging Spectroradiometer (MODIS) is an optical sensor onboard the Terra and Aqua satellites as part of the NASA Earth Observing System. MODIS scans the entire Earth surface every 1–2 days, acquiring data in 36 spectral bands. Out of the 36 spectral bands, 7 bands are designed for the study

of vegetation and land surfaces: blue (459–479 nm), green (545–565 nm), red (620–670 nm), near infrared (NIR1: 841–875 nm, NIR2: 1230–1250 nm), and shortwave infrared (SWIR1: 1628–1652 nm, SWIR2: 2105–2155 nm). Daily global imagery is provided at spatial resolutions of 250 m (red and NIR1) and 500 m (blue, green, NIR2, SWIR1, and SWIR2). The MODIS Land Science Team provides a suite of standard MODIS data products to users, including the Surface Reflectance 8-Day L3 Global 500 m product (MOD09A1). There are forty-six 8-day composites in a year, starting with January 1st each year. The MOD09A1 data are organized in tile fashion and freely available to the public from the US Geological Survey EROS Data Center (USGS EDC, http://edc.usgs.gov).

The MOD09A1 datasets, which have a 500-m spatial resolution and 8-day temporal resolution, were downloaded from the USGS EDC website using the geographic location of each flux tower, and time-series of land surface reflectance were extracted. This produced a time series record of land surface reflectance for a single pixel over each flux tower site. The MOD09A1 data files have quality flags for all observations, including cloud and shadow flags. Cloudy observations within a year were identified and gap-filled, following the procedure described in earlier studies (Xiao et al., 2005a and Xiao et al., 2006). Additionally, an observation with a blue band reflectance ≥0.2 during the growing season was also treated as a poor-quality observation and gap-filled. Due to an instrument calibration task, MODIS observations in 2001 are missing one 8-day period (18–25 June 2001, the 22nd 8-day composite); no image was acquired. To address this, a blank period (22nd observation) was inserted between the 21st observation (10–17 June 2001) and 23rd observation (26 June–3 July 2001), and this blank was gap-filled using a linear function and data from the 21st and 23rd observations.

For each MODIS 8-day composite, three vegetation indices were calculated: (1) the Normalized Differential Vegetation Index (NDVI; (Tucker, 1979)), (2) the Enhanced Vegetation Index (EVI; (Huete et al., 1997 and Huete et al., 2002)), and (3) the Land Surface Water Index (LSWI; (Xiao et al., 2004a and Xiao et al., 2005b)), using surface reflectance (ρ) from the blue, green, red, NIR1, and SWIR1 bands (Equations (1)–(3)). These three indices are used in a number of large-scale agricultural studies (Xiao et al., 2005a, Xiao et al., 2006, Sims et al., 2008, Gwathmey et al., 2010 and Wen et al., 2010).

$$NDVI = \frac{\rho_{NIR1} - \rho_{red}}{\rho_{NIR1} + \rho_{red}} \tag{1}$$

$$EVI = \frac{2.5 \times \rho_{NIR1} - \rho_{red}}{\rho_{NIR1} + 6 \times \rho_{red} - 7.5 \times \rho_{blue} + 1} \tag{2}$$

$$LSWI = \frac{\rho_{NIR1} - \rho_{SWIR1}}{\rho_{NIR1} + \rho_{SWIR1}} \tag{3}$$

2.4. The Vegetation Photosynthesis Model

2.4.1. Model structure

Leaves and canopies are composed of photosynthetically active vegetation (mostly chlorophyll) and non-photosynthetic vegetation (NPV; mostly cell walls, senescent foliage, branches, stems, and trunks). Accordingly, the fraction of photosynthetically active radiation (PAR) absorbed by the vegetation canopy ($FPAR_{canopy}$) is partitioned into the fraction absorbed by chlorophyll ($FPAR_{chl}$) and the fraction absorbed by NPV ($FPAR_{NPV}$). Only light absorbed by chlorophyll (a product of PAR × $FPAR_{chl}$) is used for photosynthesis.

Based on this conceptual partitioning of $FPAR_{chl}$ and $FPAR_{NPV}$ within the canopy, the Vegetation Photosynthesis Model was developed to estimate GPP of vegetation over the growing season (Xiao et al., 2004a):

$$GPP = PAR \times FPAR_{chl} \times \varepsilon_g \tag{4}$$

Table 3. Dates of important cultivation events at the five study sites in Nebraska and Minnesota, U.S.A. The planting, emergence, and harvest dates were directly observed in the field, while the Start and End dates where LSWI ≥ −0.1 were obtained from the date stamp of the image used in the MOD09A1 8-day composites. The 8-day period number (in parentheses) in a year follows the exact image date.

| Year	Planting date	Emergence date	Harvest date	LSWI ≥ −0.1 Start date	End date
Mead Irrigated					
2001	10-May	no data	18-Oct	10-Jun (21)	14-Oct (36)
2002	9-May	no data	4-Nov	6-Jun (20)	10-Oct (36)
2003	15-May	no data	27-Oct	16-Jun (21)	6-Oct (35)
2004	3-May	no data	14-Oct	4-Jun (20)	29-Sep (35)
2005	4-May	no data	12-Oct	7-Jun (20)	27-Sep (34)
Mead Irrigated Rotation					
2001	11-May	18-May	22-Oct	10-Jun (21)	14-Oct (36)
2003	15-May	25-May	23-Oct	16-Jun (21)	6-Oct (35)
2005	2-May	no data	17-Oct	7-Jun (20)	27-Sep (34)
Mead Rainfed					
2001	14-May	no data	29-Oct	1-Jun (19)	14-Oct (36)
2003	13-May	no data	13-Oct	31-May (19)	15-Sep (33)
2005	26-Apr	no data	17-Oct	27-May (19)	2-Oct (35)
Rosemount G19					
2005	3-May	no data	20-Oct	16-Jun (21)	15-Oct (36)
Rosemount G21					
2005	3-May	no data	29-Oct	7-Jun (20)	15-Oct (36)
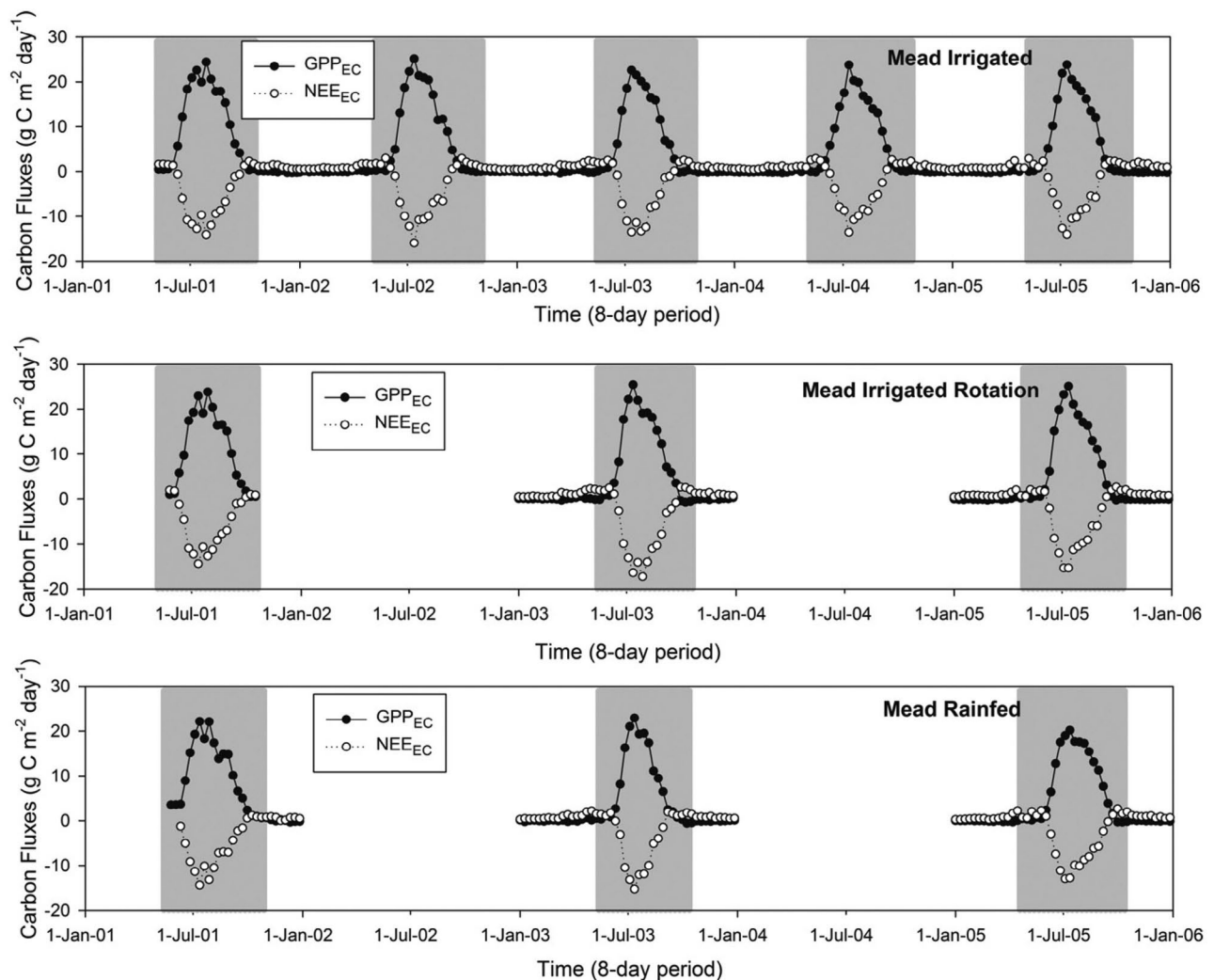
Figure 3. Seasonal dynamics and interannual variation of observed net ecosystem exchange (NEE_{EC}) of CO_2 and estimated gross primary production (GPP_{EC}) for the three flux tower sites in Mead, Nebraska, U.S.A. during 2001–2005, with the cultivation periods highlighted: (a) the irrigated, continuously maize site, (b) the irrigated, annual maize–soybean rotation site, and (c) the rain-fed, annual maize–soybean rotation site.

where PAR is the photosynthetically active radiation (μmol photosynthetic photon flux density, PPFD), FPAR$_{chl}$ is the fraction of PAR absorbed by leaf chlorophyll in the canopy, and ε_g is the light-use efficiency (μmol CO$_2$ μmol PPFD^{-1}).

2.4.2. Model parameter estimation

In the VPM, FPAR$_{chl}$ within the photosynthetically active period of vegetation is estimated as a linear function of EVI, and the coefficient a is set to be 1.0 (Xiao et al., 2004a, 2004b):

$$\text{FPAR}_{chl} = a \times \text{EVI} \tag{5}$$

Light-use efficiency (ε_g) is affected by temperature, water, and leaf phenology:

$$\varepsilon_g = \varepsilon_0 \times T_{scalar} \times W_{scalar} \times P_{scalar} \tag{6}$$

where ε_0 is the apparent quantum yield or maximum light-use efficiency (μmol CO$_2$ μmol PPFD^{-1}), and T_{scalar}, W_{scalar}, and P_{scalar} are the scalars for the affects of temperature, water, and leaf phenology, respectively, on the maximum light-use efficiency of vegetation (Xiao et al., 2004a, 2005b).

The maximum light-use efficiency (ε_0) parameter value varies dependent upon biome type and the method of parameter estimation used (Xiao, 2006). In previous studies using the VPM, the ε_0 parameter value was derived using hourly NEE data and incident PAR data from a flux tower site over a period of time (e.g., 1–2 weeks long) within the peak of the plant growing-season (Wofsy et al., 1993; Yan et al., 2009; Wang et al., 2010b). In this study a theoretical ε_0 value (0.125 mol CO$_2$ mol PPFD^{-1} or 1.5 g C mol PPFD^{-1}) reported in an early study of CO$_2$ exchange and quantum yield of photosynthesis (Emerson and Lewis, 1941) was used.

There are a number of ways to estimate the effect of temperature on photosynthesis (T_{scalar}). In the VPM, T_{scalar} is estimated at each time step, using the equation developed for the Terrestrial Ecosystem Model (Raich et al., 1991):

$$T_{scalar} = \frac{(T - T_{min})\,(T - T_{max})}{[(T - T_{min})\,(T - T_{max})] - (T - T_{opt})^2} \tag{7}$$

where T_{min}, T_{opt}, and T_{max} are the minimum, optimum, and maximum temperature for photosynthetic activities, respectively. If air temperature falls below T_{min}, T_{scalar} is set to zero. T_{min}, T_{opt}, and T_{max} parameters vary depending on the photosynthetic pathway (e.g., C$_3$ vs. C$_4$) and on the vegetation type (e.g. maize vs. sugarcane). Temperature changes due to variations such as season, altitude, and the diurnal cycle introduce complex, plant-specific (and in some cases leaf-specific) adaptations (Berry and Björkman, 1980). Choosing a broad temperature range widely applicable to various cases prevents models from becoming plant, specie, or canopy-height specific. As opposed to arriving at a temperature range specific to maize grown in the 'Corn Belt' or generally applicable to all maize, a temperature range accommodating many C$_4$ plants was used. Most physiological processes for plants range from 0 to 40 °C (Went, 1953), with growth under a cool or warm regime improving photosynthetic performance at low or high temperatures, respectively (Berry and Björkman, 1980). However, C$_4$ species often exhibit sensitivity to temperatures below 10 °C (Sugiyama, 1973), with maize largely senescent when air temperature is ≤10 °C (Verma et al., 2005). C$_4$ species possess advantages for growth in warm climates compared to C$_3$ species, extending the temperature range for growth up to 48 °C for many C$_4$ species and 50 °C for a few species native to hot, tropical environments (Sage and Monson, 1999). Crafts-Brandner and Salvucci (2002) found a broad temperature optimum for maize existing between 28 and 37.5 °C, and similar C$_4$ temperature optimums have been found by others (Went, 1953; Hirasawa and Hsiao, 1999; Kubien et al., 2003; Kim et al., 2007; Osborne et al., 2008). Considering optimum

temperature ranges and the predominant climate at the flux tower sites, the T_{min}, T_{opt}, and T_{max} parameter values are set to 10, 28, and 48 °C, respectively, for this study.

The VPM uses the satellite-derived Land Surface Water Index (LSWI) to estimate the effect of water on photosynthesis (W_{scalar}):

$$W_{scalar} = \frac{1 + \text{LSWI}}{1 + \text{LSWI}_{max}} \tag{8}$$

where LSWI$_{max}$ is the maximum LSWI during the growing season for individual pixels. The maximum LSWI value within the growing season is selected as an estimate of LSWI$_{max}$ (Xiao et al., 2004a, 2005b), with estimation of site-specific LSWI$_{max}$ dependent upon the time series of remotely sensed data. For maize, each cultivation period at each site has a unique LSWI$_{max}$, since the lifecycle of maize is one cultivation period, and this was used for simulations.

In the VPM, P_{scalar} is included to account for the effect of leaf age on photosynthesis at the canopy level, and calculation of P_{scalar} is dependent upon leaf longevity. Equation (9) is used for deciduous forests, which have a distinct green-up period (1–2 weeks long), and Equation (10) is used for evergreen forests, grasslands, and crops.

$$P_{scalar} = \frac{1 + \text{LSWI}}{2} \quad \text{From emergence to complete leaf-expansion} \tag{9}$$

$$P_{scalar} = 1 \quad \text{After complete leaf-expansion} \tag{10}$$
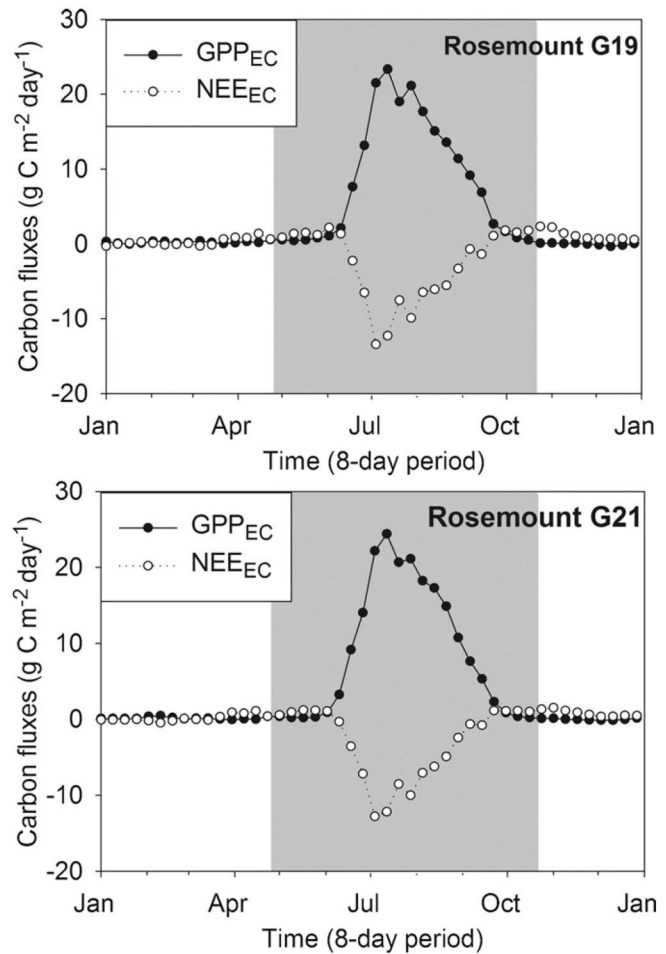

Figure 4. Seasonal dynamics and interannual variation of observed net ecosystem exchange (NEE$_{EC}$) of CO$_2$ and estimated gross primary production (GPP$_{EC}$) for the two flux tower sites in Rosemount, Minnesota, U.S.A. during 2005, with the cultivation periods highlighted: (a) the Rosemount G19 site and (b) the Rosemount G21 site.

3. Results

In order to compare GPP$_{EC}$ and GPP$_{VPM}$, the time period for such a comparison must first be defined. Three possible periods were described in Section 2.1. Of these three periods, the crop-growth period is the most appropriate. The cultivation period is obviously longer than the crop-growth period, as seeds often take weeks to emerge and farmers often harvest crops weeks after crops enter senescence. Using the cultivation period could result in biased or skewed results by including many near-zero data points from before crop emergence and after crop senescence. All statistical analyses completed in this study are conducted using the crop-growth period.

3.1. Seasonal dynamics of CO$_2$ flux and land surface phenology

Planting, emergence, and harvest dates are shown in Table 3, with the beginning and ending of cultivation periods for each year delimited by the 8-day periods coinciding with planting and harvest, respectively.

3.1.1. The Mead sites (Mead, Nebraska)

At the Mead Irrigated Rotation site, planting occurred on 11 May 2001 and 15 May 2003 (Table 3). Field observations at this site

showed that it took 8–10 days for seed to germinate and emerge. Crop emergence at the other two Mead sites was estimated to have occurred within 2 weeks of planting by using the known Mead Irrigated Rotation emergence dates as proxies.

The seasonal dynamics of GPP and NEE observed by the eddy covariance flux towers (GPP$_{EC}$ and NEE$_{EC}$, respectively) at all three Mead sites are comparable, due to the high similarity of climatic factors (Figure 1). By early June, changes in NEE$_{EC}$ (>1 g C m^{-2} day^{-1}) were observed (Figure 3). Both GPP$_{EC}$ and NEE$_{EC}$ rose rapidly and reached a peak in July. By late September, GPP$_{EC}$ and NEE$_{EC}$ approached zero, indicative of senescent leaves, and remained at this level until harvest. Harvest at these sites occurred in mid- to late October. After harvest both GPP$_{EC}$ and NEE$_{EC}$ remained near zero throughout the winter. The crop-growth period for maize, as delineated by seasonal GPP$_{EC}$, occurs from early June to late September. Even with differences in irrigation and crop rotation practices between sites, the only observable difference among the sites is in the magnitude of GPP$_{EC}$ and NEE$_{EC}$. The Mead Irrigated Rotation site exhibits the greatest flux magnitude, followed by the Mead Irrigated site and then the Mead Rainfed site.

3.1.2. The Rosemount sites (St. Paul, Minnesota)

Planting at these sites occurred on 3 May 2005 (Table 3). No specific crop emergence dates were reported for these sites. By early June, changes in NEE$_{EC}$ (>1 g C m^{-2} day^{-1}) were observed
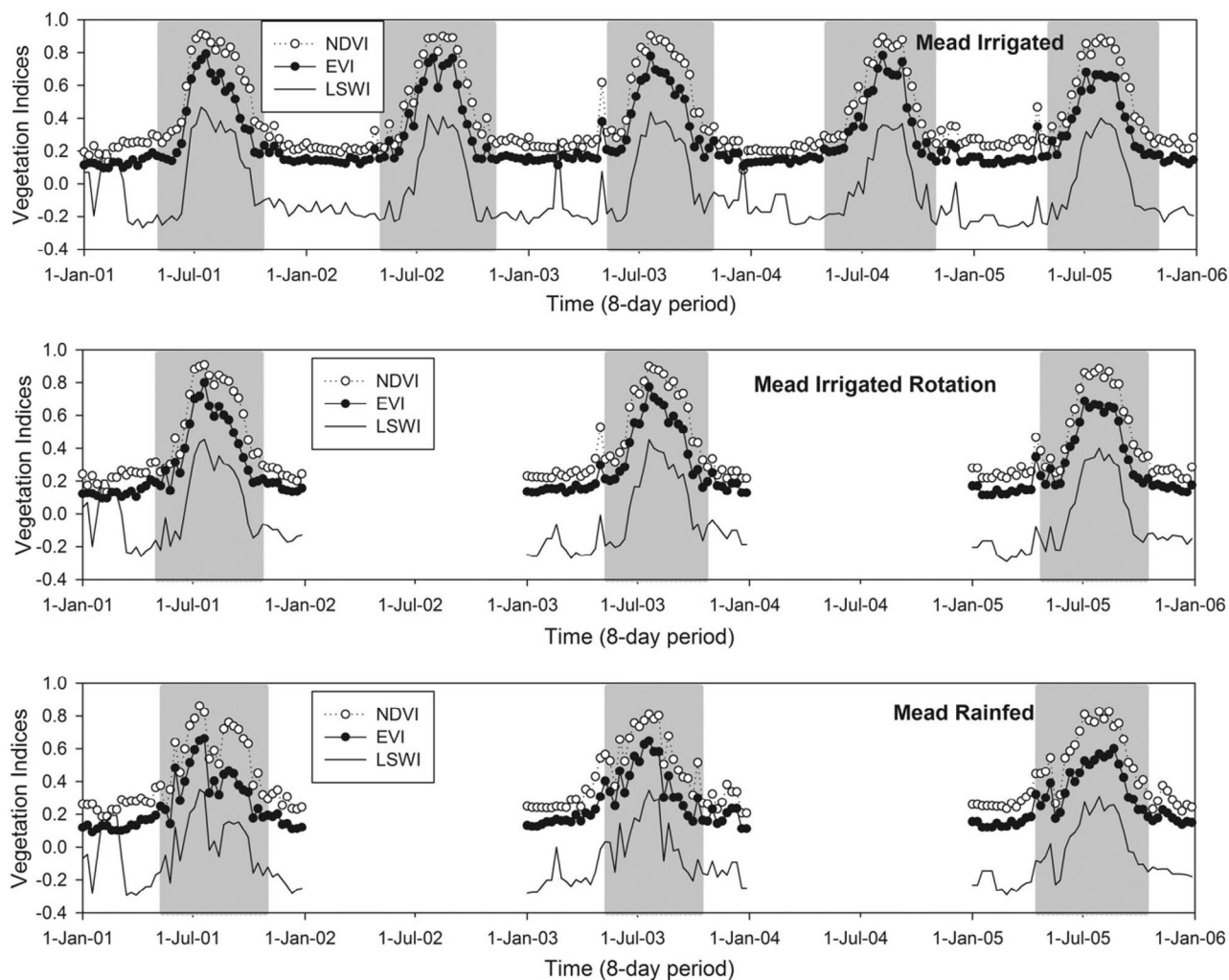

Figure 5. Seasonal dynamics and interannual variation of three vegetation indices for the three maize sites in Mead, Nebraska, U.S.A. during 2001–2005, with the cultivation periods highlighted: (a) the irrigated, continuously maize site, (b) the irrigated, annual maize–soybean rotation site, and (c) the rain-fed, annual maize–soybean rotation site.

(Figure 4). GPP_EC and NEE_EC rose rapidly and reached a peak in early July. After the seasonal peak, both GPP_EC and NEE_EC declined rapidly and approached zero by October, indicative of senescent leaves, and remained at this level until harvest, which occurred on 15 October. After harvest, both GPP_EC and NEE_EC remained near zero throughout the winter. The growing-season for maize, as delineated by seasonal GPP_EC, occurs from early June to late September.

3.2. Seasonal dynamics of vegetation indices and land surface phenology

In this study, the dynamics of vegetation indices within the cultivation period (generally May–October, see Table 3) were analyzed to characterize their performance for identifying crop phenology.

3.2.1. The Mead sites (Mead, Nebraska)

After planting, NDVI, EVI, and LSWI values remained relatively low for a few 8-day periods but rose rapidly in early June (Figure 5), which corresponded well with the timing of GPP_EC and NEE_EC data in early summer (Figure 3). This suggests that all three vegetation indices are useful indicators for cropland phenology, specifically for identifying and tracking the starting dates of crop-growth periods. The threshold values for NDVI, EVI and LSWI, when both GPP_EC and NEE_EC had discernable changes (>1 g C m^{-2} day^{-1}) in early summer, were ≥0.3, ≥0.2, and ≥−0.1, respectively (Figure 5). NDVI, EVI and, LSWI reached peak values in July and then declined to low values by late September to early October, which also corresponded well with the timing of GPP_EC and NEE_EC (Figure 3). The threshold values for NDVI, EVI and LSWI, when both GPP_EC and NEE_EC remained near zero in the fall, were ≤0.3, ≤0.2, and ≤−0.1, respectively (Figure 5). For the Mead sites, the vegetation indices indicated that the crop-growth period was approximately from the first week in June to the end of September, matching GPP_EC well, but this interval is over a month shorter than the cultivation period (Table 3).

The peak values of NDVI, EVI, and LSWI at the two irrigated Mead sites were only slightly higher than those at the Mead Rainfed site (Figure 5), although the amounts of seeds sown at the Mead Rainfed site were 25–35% smaller than the other two sites. For example, the NDVI maximum was >0.9 at the irrigated sites but 0.8–0.9 at the rain-fed site. Slightly lower NDVI and EVI values across the entire crop-growth period in all years at the Mead Rainfed site are attributed to the relatively decreased crop density of this field; however, they are also partly attributed to water stress observed 5 days in 2001 and 32 days in 2003 at the Mead Rainfed site (Verma et al., 2005).

3.2.2. The Rosemount sites (St. Paul, Minnesota)

NDVI, EVI, and LSWI values were slightly higher after planting than before planting (Figure 6). NDVI, EVI, and LSWI values rose rapidly in mid-June, which corresponded well with the timing of GPP_EC and NEE_EC in early summer (Figure 4). The threshold values for NDVI, EVI, and LSWI where GPP_EC and NEE_EC significantly changed (>1 g C m^{-2} day^{-1}) in early summer were ≥0.3, ≥0.2, and ≥−0.1, respectively (Figure 6).

The three vegetation indices reached their peak values in July, remained at that level through August, and declined rapidly in early September. The threshold values for NDVI, EVI, and LSWI, when GPP_EC and NEE_EC returned to near zero in the fall, were ≤0.3, ≤0.2, and ≤−0.1, respectively (Figure 6). The crop-growth period, as defined by both vegetation indices and GPP_EC, was approximately from early June to early October.

3.3. Quantitative relationships between vegetation indices and GPP_EC

Simple linear regressions between vegetation indices (NDVI and EVI) and GPP_EC during the crop-growth period (where LSWI ≥ −0.1) were calculated for each site (Figure 7 and Figure 8). NDVI accounted for 55% (Mead Irrigated), 71% (Mead Irrigated Rotation), and 59% (Mead Rainfed) of GPP_EC variances at the Mead sites (Figure 7). NDVI also accounted for 74% (Rosemount G19) and 71% (Rosemount G21) of GPP_EC variances at the Rosemount sites (Figure 8). EVI has a slightly stronger linear relationship with GPP_EC than does NDVI at the Mead sites. The relationship between NDVI and GPP_EC has a curvilinear scatter at all sites that can be attributed to NDVI saturation in dense canopies (Huete et al., 1997). As crop canopy approached full maturity, EVI was more able to detect subtle canopy density increases. This was evident at the Mead sites where best management practices were implemented, producing greater yields and higher nitrogen efficiencies than in average production fields (Verma et al., 2005) and where the Mead Irrigated and Mead Irrigated Rotation sites had greater crop densities compared to the Mead Rainfed site.

3.4. Seasonal dynamics of GPP predicted by the Vegetation Photosynthesis Model (GPP_VPM)

Pearson product-moment correlations between GPP_EC and GPP_VPM were completed for each site using data within the crop-growth
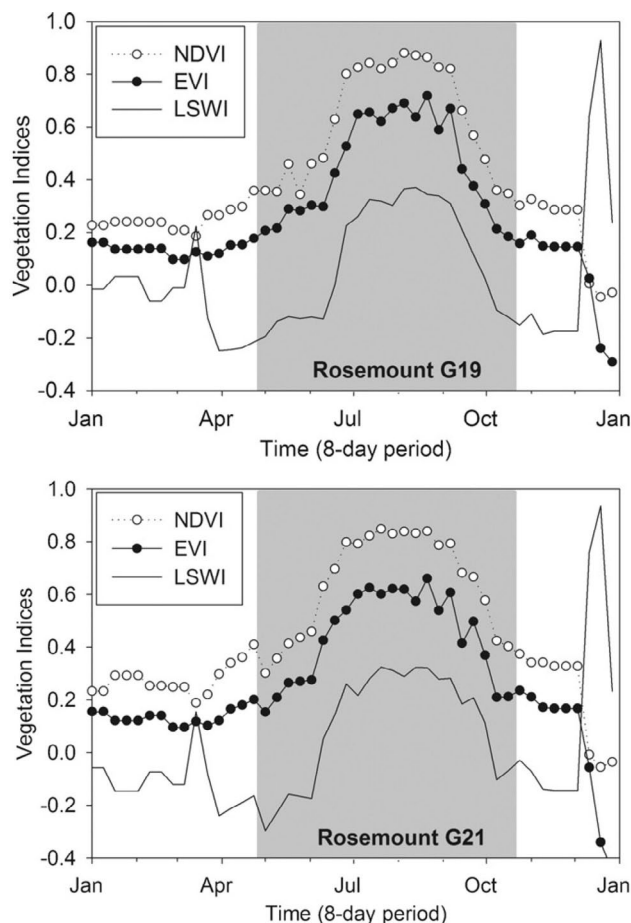

Figure 6. Seasonal dynamics and interannual variation of three vegetation indices for the two maize sites in Rosemount, Minnesota, U.S.A. during 2005, with the cultivation periods highlighted: (a) the Rosemount G19 site and (b) the Rosemount G21 site.
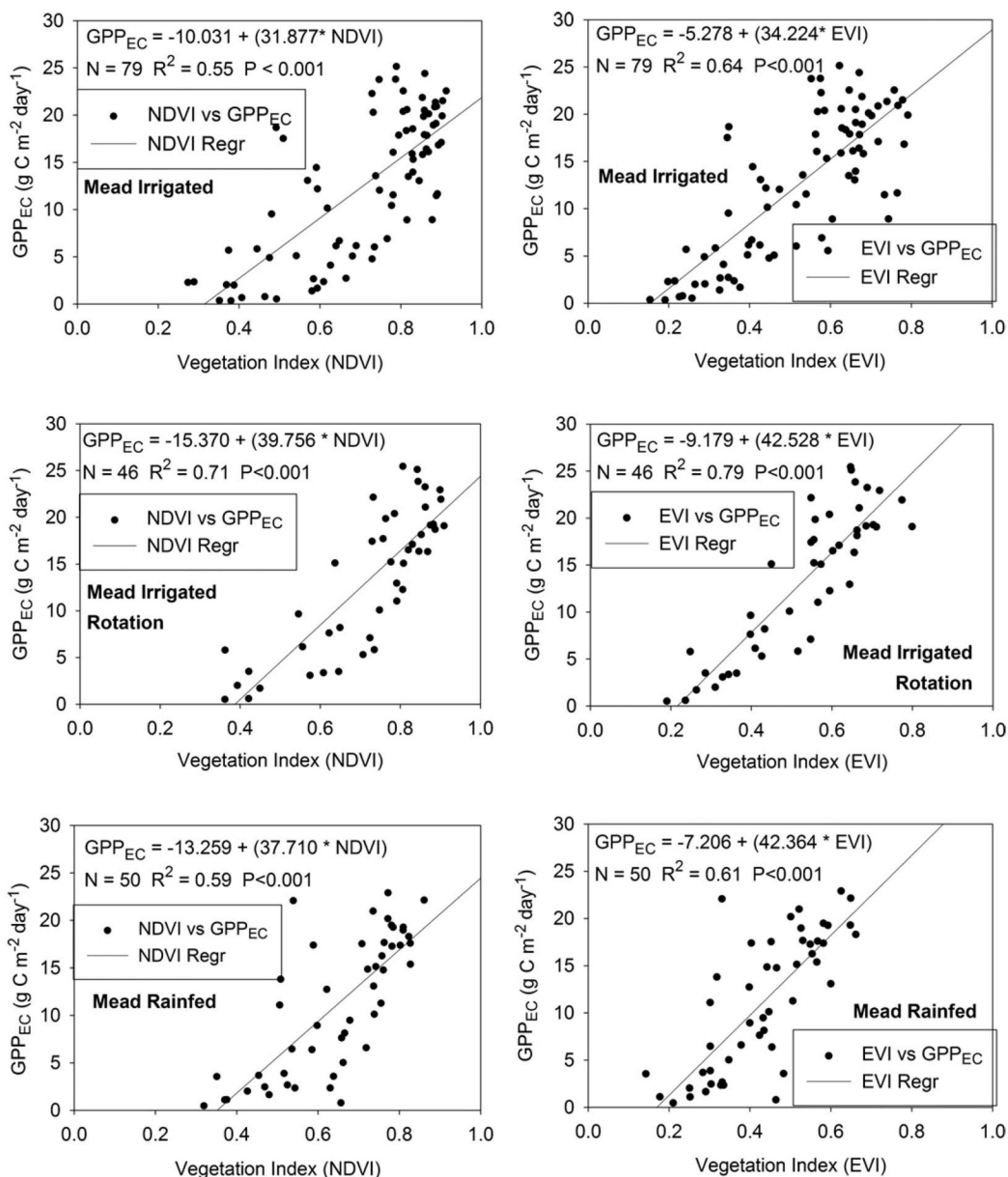
Figure 7. A comparison between estimated gross primary production (GPP$_{EC}$) and vegetation indices (NDVI and EVI) during the crop-growth period (where LSWI ≥ −0.1) for the three sites in Mead, Nebraska, U.S.A.: (a) the irrigated, continuously maize site, (b) the irrigated, annual maize–soybean rotation site, and (c) the rain-fed, annual maize–soybean rotation site.

period, along with calculations of Root Mean Square Deviation (RMSD) and percent relative error (%RE) for seasonal (crop-growth period) sums of GPP.

3.4.1. The Mead sites (Mead, Nebraska)

The seasonal dynamics of GPP$_{EC}$ estimates were compared with GPP predicted by the VPM (GPP$_{VPM}$) for the three Mead sites (Figure 9). As with GPP$_{EC}$, GPP$_{VPM}$ exhibits temporal characteristics consistent across all sites and years. During May (after planting until shortly after emergence) GPP$_{VPM}$ values were higher than GPP$_{EC}$. Once the crop-growth period begins, GPP$_{VPM}$ tracks GPP$_{EC}$ well throughout the crop-growth period and until the cultivation period ends. GPP$_{VPM}$ rises abruptly in early June, matching the GPP$_{EC}$ rise. The seasonal peaks of GPP$_{VPM}$ also match the seasonal peaks of GPP$_{EC}$ that occurred in July. GPP$_{VPM}$ values approached zero by late September and remained near zero until harvest, matching the trends in GPP$_{EC}$ and corresponding to the timing of the end of

both the crop-growth period and the cultivation period.

The scatterplots between GPP$_{VPM}$ and GPP$_{EC}$ over the crop growth period (Figure 10) show the Mead Irrigated Rotation site has the highest Pearson product-moment correlation coefficient (r = 0.96; 3 years), followed by the Mead Irrigated site (r = 0.89; 5 years) and the Mead Rainfed site (r = 0.88; 3 years). As shown in Table 4, the Mead Irrigated site has the largest interannual variations of root mean square deviation (RMSD) values, which ranged from 1.56 g C m^{-2} d^{-1} in 2001 to 5.62 g C m^{-2} d^{-1} in 2004. RMSD values in 2002 and 2004 at the Mead Irrigated site are significantly larger than the other years (2001, 2003 and 2005).

Table 4 also compares the seasonal sums of GPP over the crop growth period between GPP$_{EC}$ and GPP$_{VPM}$ at three Mead sites (a total of 11 site-years). When excluding the year 2003 in the Mead Irrigated site and the year 2001 in the Mead Rainfed site, the remaining 9 site-years have a percent relative error (%RE) from −9% to 5% between GPP$_{EC}$ and GPP$_{VPM}$ (Table 4).
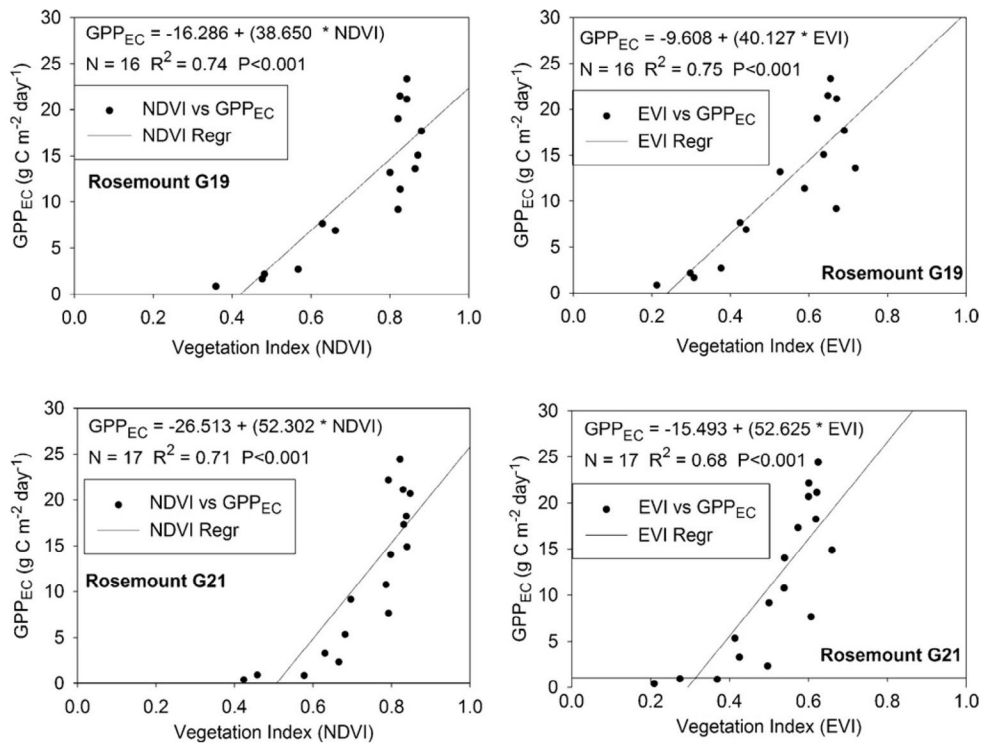
Figure 8. A comparison between estimated gross primary production (GPP_{EC}) and vegetation indices (NDVI and EVI) during the crop-growth period (where LSWI ≥ −0.1) for the two sites in Rosemount, Minnesota, U.S.A.: (a) the Rosemount G19 site and (b) the Rosemount G21.

3.4.2. The Rosemount sites (St. Paul, Minnesota)

Figure 11 shows the seasonal dynamics of GPP_{EC} and GPP_{VPM} at the two Rosemount sites. Between the planting date and the beginning of the crop-growth period, GPP_{VPM} were higher than GPP_{EC}. Although GPP_{VPM} was slightly higher for approximately 1 month past the start of the crop-growth period, GPP_{VPM} at both sites increased rapidly and reached seasonal peaks in July, corresponding well with GPP_{EC} timing once the crop-growth period commenced. GPP_{VPM} returns to values near zero by October.

The scatterplots between GPP_{EC} and GPP_{VPM} over the crop-growth period at the two Rosemount sites show that GPP_{EC} and GPP_{VPM} are strongly correlated with each other (Figure 12). The correlation coefficient was 0.98 at the Rosemount G19 site

and 0.94 at the Rosemount G21 site. The RMSD value in 2005 is 1.42 g C m^{-2} d^{-1} for the Rosemount G19 site, which is lower than those in 2005 at the Mead sites. The Rosemount G21 site has a RMSD value of 3.09 g C m^{-2} d^{-1} in 2005, which is higher than those in 2005 at the Mead sites (Table 4).

As shown in Table 4, the seasonal sums of GPP_{VPM} during the crop-growth period in 2005 were 1610 and 1615 g C m^{-2} at the Rosemount G19 and Rosemount G21 sites, which are about 7.83% and 4.49% higher than the seasonal sum of GPP_{EC}, respectively. The %RE between GPP_{EC} and GPP_{VPM} over the crop-growth period in 2005 at the Rosemount sites are in similar range to those at the Mead sites (Table 4).

Table 4. Seasonal sums and statistics of gross primary production (GPP) for the five study sites in Nebraska and Minnesota, U.S.A. RMSD: root mean squared deviation; GPP_{EC}: seasonal sum of GPP estimated from eddy covariance flux tower observations in g C m^{-2}; GPP_{VPM}: seasonal sum of GPP predicted by the VPM in g C m^{-2}: GPP %RE: relative error in GPP sums calculated as [(GPP_{EC} − GPP_{VPM})/GPP_{EC}] × 100.

| Year	RMSD	GPP_{EC} (g C m^{-2})	GPP_{VPM} (g C m^{-2})	GPP %RE
Mead Irrigated				
2001	1.56	1743	1660	4.74
2002	4.40	1648	1676	−1.65
2003	2.37	1461	1685	−15.35
2004	5.62	1516	1461	3.64
2005	2.08	1505	1640	−8.97
Mead Irrigated Rotation				
2001	1.18	1657	1589	4.12
2003	2.95	1589	1734	−9.12
2005	1.93	1599	1721	−7.66
Mead Rainfed				
2001	4.67	1620	1294	20.09
2003	2.89	1283	1392	−8.57
2005	2.18	1468	1546	−5.28
Rosemount G19				
2005	1.42	1493	1610	−7.83
Rosemount G21				
2005	3.09	1546	1615	−4.49
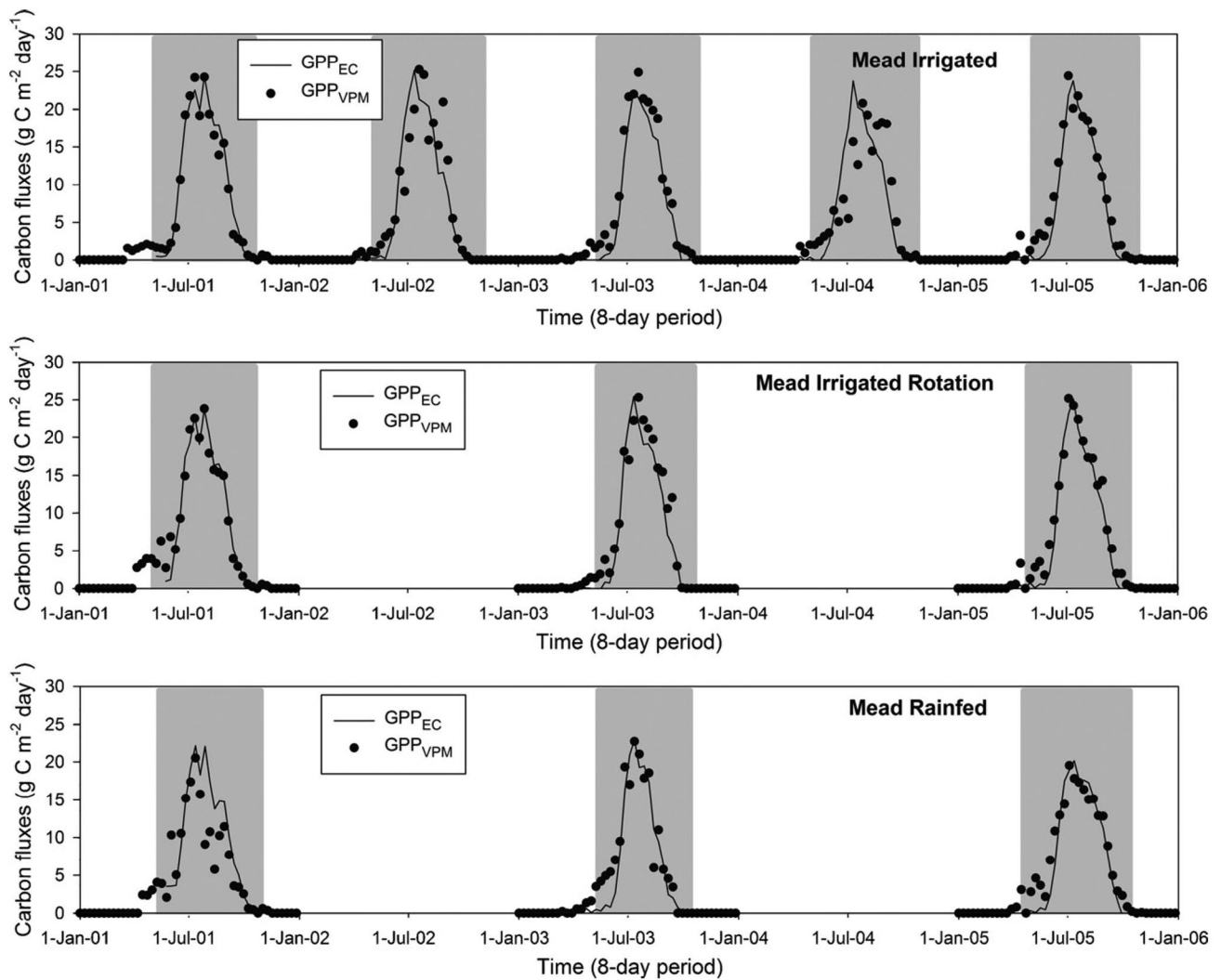
Figure 9. Seasonal dynamics and interannual variation of gross primary production estimates from the flux towers (GPP$_{EC}$) and the VPM-predicted gross primary production (GPP$_{VPM}$) for the three maize sites in Mead, Nebraska, U.S.A. during 2001–2005, with the cultivation periods highlighted: (a) the irrigated, continuously maize site, (b) the irrigated, annual maize–soybean rotation site, and (c) the rain-fed, annual maize–soybean rotation site.

4. Discussion

The biophysical performance of vegetation indices (e.g., NDVI and EVI) is important as vegetation indices are often used to estimate leaf area index (LAI), FPAR$_{canopy}$, FPAR$_{chl}$, GPP, and biomass (Huete et al., 2002, Frank and Karn, 2003, Zhang et al., 2005, Zhang et al., 2006a, Yuan et al., 2007, Wu et al., 2010a and Yuan et al., 2010). In comparison to NDVI, EVI was found to be more linearly correlated with green leaf area index (LAI) in crop fields (Boegh et al., 2002), less prone to saturation in temperate and tropical forests (Xiao et al., 2004a and Huete et al., 2006), and less sensitive to residual aerosol contamination from extensive fires (Xiao et al., 2003). However, vegetation indices can be affected by topography in addition to atmospheric conditions and soil background. In landscape of complex topography, e.g., mountainous areas, topography may have different effects on NDVI and EVI. The soil adjustment factor in EVI prevents EVI from being expressed as a function of the ratio vegetation index, causing EVI to be subject to topographic effects and to be subject to changes in brightness caused by target area per pixel distortions, things that are absolutely reduced in NDVI (Matsushita et al., 2007). The maize sites of this study were located in flat plain areas, with the effect of topography minimal and negligible, and results showed that EVI has

a stronger linear relationship with GPP$_{EC}$ than does NDVI for irrigated maize sites, consistent with the results of previous studies for other biome types, including deciduous broadleaf forests (Xiao et al., 2004b and Wu et al., 2009), evergreen needle-leaf forest (Xiao et al., 2005b), and grassland and wheat cropland (Yan et al., 2009 and Wu et al., 2010b). The VPM was the first model that used EVI as an estimate of FPAR$_{chl}$ within the photosynthetically active period of vegetation to estimate GPP, and EVI has recently been used in several other LUE models that estimate GPP (Sims et al., 2006, Sims et al., 2008 and Wu et al., 2010c). Although care must be taken to use satellite-derived indices appropriately, the results demonstrated a value of using EVI in agricultural studies.

Information on crop calendar (e.g., planting date, harvest date) and crop phenology is important for crop management and yield estimation as well as understanding the carbon cycle dynamics (Jans et al., 2010; Moors et al., 2010). For maize plants, a distinct leaf expansion phase can be identified over the cultivation period. Maize phenology is thus generally divided into (1) vegetative (from emergence to tasseling according to the number of fully expanded leaves), (2) reproductive (from silking to physiological maturity according to the degree of kernel development) and (3) senescence stages (Ritchie et al., 1992; Vina et al., 2004). Spectral data and vegetation indices have been used to track maize crop
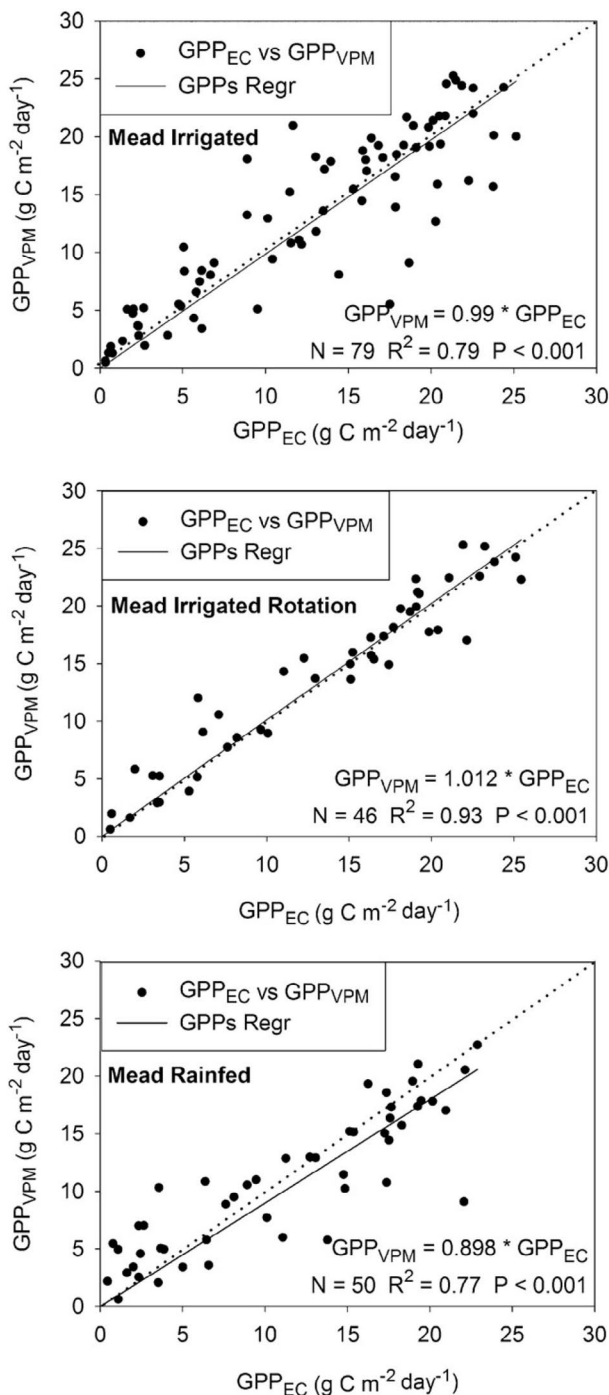
Figure 10. A scatterplot comparison between estimated gross primary production (GPP_{EC}) and predicted gross primary production (GPP_{VPM}) at the three maize sites in Mead, Nebraska, U.S.A.: (a) the irrigated, continuously maize site, (b) the irrigated, annual maize–soybean rotation site, and (c) the rain-fed, annual maize–soybean rotation site.

Figure 11. Seasonal dynamics and interannual variation of gross primary production estimates from the flux towers (GPP_{EC}) and the VPM-predicted gross primary production (GPP_{VPM}) for the two maize sites in Rosemount, Minnesota, U.S.A. during 2005, with the cultivation periods highlighted: (a) the Rosemount G19 site and (b) the Rosemount G21 site.

development, including (1) the onset of green-up and (2) the onset of senescence (Tucker et al., 1979; Vina et al., 2004). In this study, three vegetation indices were evaluated for their potential to delineate maize phenology in the context of CO_2 flux dynamics. The threshold values of NDVI (0.3), EVI (0.2) and LSWI (−0.1) found for the sites in this study are similar to values observed at a maize site in North China (Yan et al., 2009). While NDVI and EVI time-series data are widely used in delineating land surface phenology (Zhang et al., 2003, Boles et al., 2004, de Beurs and Henebry,
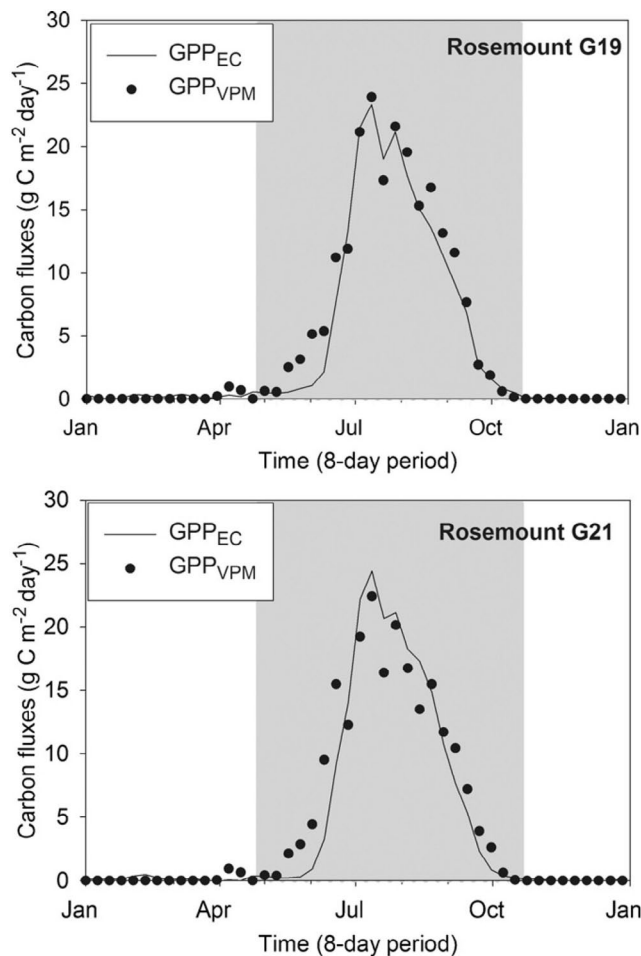
2004 and Zhang et al., 2006b), the results of this study show the potential of using LSWI time series data to delineate maize phenology. LSWI values were < −0.2 prior to the known planting dates for these sites and had the greatest consistency across all sites immediately prior to harvest, having values ≤ −0.1 and in some cases ≤ −0.2 (Figure 5 and Figure 6). Considering agricultural practices, seasonal timing, and crop phenology, LSWI values ≤ −0.1 are attributed here to minimally productive vegetated surfaces (plant emergence or crop senescence) while LSWI values ≤ −0.2 are attributed to bare fields.

Discrepancies between GPP_{VPM} and GPP_{EC} at the five maize sites in this study are relatively small and reasonable (Table 4). Out of the 13 site-years at the Mead and Rosemount sites (Table 4), 11 site-years had a <10% discrepancy between the seasonal sums of GPP_{VPM} and GPP_{EC}. There is a need to further investigate the relatively large discrepancies in 2003 at the Mead Irrigated site and 2001 at the Mead Rainfed site. Among the five flux tower sites (Table 2), only the Rosemount G21 site has a crop field extent that is smaller than a single MODIS pixel (500-m spatial resolution in the MOD09A1 dataset), and is surrounded by deciduous trees and grasslands. Mixed pixels are a common problem in the use of moderate resolution satellite images, and additional years of observations at the Rosemount G21 site are needed to better assess the effect of mixed pixels on CO_2 flux measurements and VPM simulations.
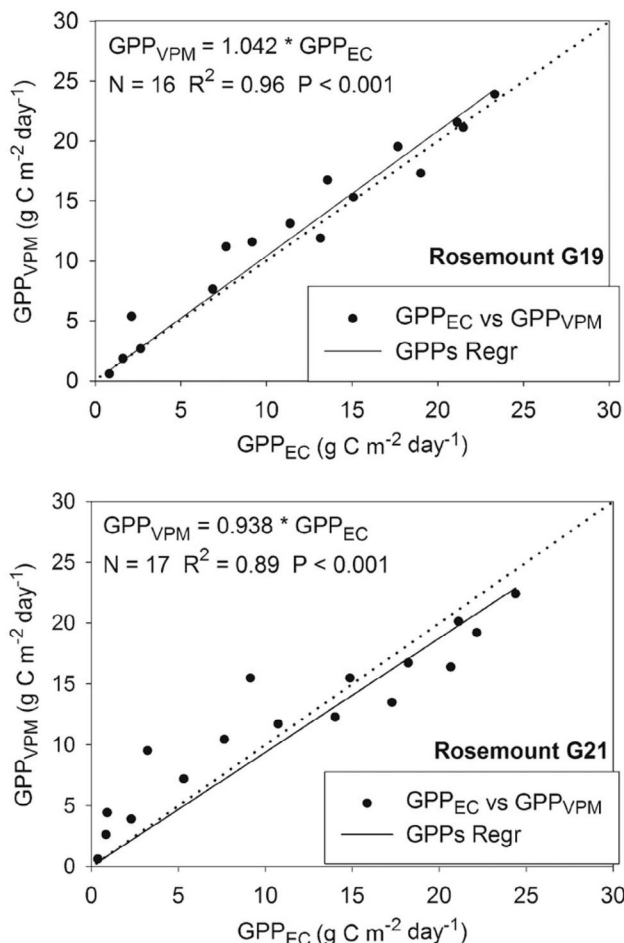
Figure 12. A scatterplot comparison between estimated gross primary production (GPP$_{EC}$) and predicted gross primary production (GPP$_{VPM}$) at the two maize sites in Rosemount, Minnesota, U.S.A.: (a) the Rosemount G19 site and (b) the Rosemount G21.

Several studies of maize based on the eddy covariance technique have reported a large variation in GPP. Peak GPP values at the five sites in this study were approximately 25 g C m^{-2} d^{-1} (Figures 3 & 4), much higher than peak GPP values (~15 g C m^{-2} d^{-1}) at three maize sites in China (Yan et al., 2009; Lei and Yang, 2010; Wang et al., 2010b; Wu et al., 2010c) and moderately higher than peak GPP values (~20 g C m^{-2} d^{-1}) at two maize sites in France (Béziat et al., 2009; Stella et al., 2009). In a previous study, the VPM was applied to two maize sites in China, and GPP$_{VPM}$ tracked well with the seasonal dynamics of GPP$_{EC}$ (Yan et al., 2009; Wang et al., 2010b). GPP$_{VPM}$ values are highly correlated with GPP$_{EC}$ in this study, regardless of water management practice (irrigation vs. rain-fed), crop density, or crop rotation system (continuously maize vs. maize and soybean rotated annually).

Maximum light-use efficiency (ε_0) is an important parameter in LUE models, whether it is variant or invariant based on vegetation types. The theoretical ε_0 of plant photosynthesis, estimated to be 0.125 mol CO$_2$ mol PPFD^{-1} or 1.5 g C mol PPFD^{-1} by Emerson and Lewis (1941), was used in this simulation, but the ε_0 parameter can be estimated using several different approaches (Ehleringer and Pearcy, 1983; Kiniry et al., 1989; Ruimy et al., 1995; Gower et al., 1999; Lobell et al., 2002; Rosati and Dejong, 2003; Bradford et al., 2005; Xiao, 2006; Gao et al., 2010; Wang et al., 2010a). The experimental values of the maximum quantum yields in C$_4$ plants under limiting light have been generally reported to be about half of the theoretical maximum (Sage and Monson, 1999), and

differences in maximum quantum yields of photosynthesis are partly attributed to variations in experimental approaches (Sinclair and Muchow, 1999; Singsaas et al., 2001). The ε_0 used in this study is much higher than the ε_0 (0.92 g C mol PPFD^{-1}) used for a maize site in the North China Plain (Yan et al., 2009) and the ε_0 (0.56 g C mol PPFD^{-1}) used for a maize site in the Northeastern China Plain (Wang et al., 2010b). Large variation in light-use efficiency parameters in GPP and NPP models clearly call for more studies of light-use efficiency for C$_4$ plants in the near future, particularly for C$_4$ croplands and C$_3$/C$_4$ mixed grassland ecosystems.

5. Conclusions

The Vegetation Photosynthesis Model, which uses the concept of light absorption by chlorophyll, was used to estimate GPP of maize, a C$_4$ photosynthetic pathway specie, in both a semi-arid environment (three flux tower sites in Nebraska) and a moist environment (two flux tower sites in Minnesota). The model used a theoretical maximum light-use efficiency (1.5 g C mol PPFD^{-1}) for all five sites in this study, which have different crop rotation systems (continuously maize vs. maize and soybean rotated annually) and water management practices (irrigation vs. rain-fed). The simulation results demonstrated the potential of using MODIS data and the VPM for estimating seasonal dynamics and interannual variation of GPP for maize cropland at an 8-day interval. The VPM is less complex than other global production efficiency models (Prince and Goward, 1995; Running et al., 2004) and has the potential to estimate GPP of maize cropland at large spatial scales across different geographic regions (e.g., the U.S.A. and China). Other flux towers exist at maize sites in distant locations across the world (Béziat et al., 2009; Stella et al., 2009; Wang et al., 2010b; Wu et al., 2010c), and it will be worthwhile to explore the convergence between land surface phenology from a remote sensing perspective and land surface phenology based on ecosystem physiology (CO$_2$ fluxes from eddy covariance measurement techniques) at other maize sites.

Expanding this study to other maize cropland and C$_4$ vegetation distributed globally where flux measurements of CO$_2$ permit outcome verification would be valuable. Other C$_4$ crops (e.g., sorghum) and grasses (e.g., switchgrass) are now used for biofuel feedstock production. The VPM could be a useful tool for tracking and estimating GPP and NPP of biofuel feedstock production sites. In addition to land use and land cover change, climate change will affect C$_4$ crops uniquely, according to CERES-Maize model results (Mera et al., 2006). Therefore, the VPM could be coupled with other crop models (e.g., DSSAT – decision support system for agrotechnology transfer) and biogeochemical models. When used in a diagnostic mode, the coupled models are likely to provide more accurate estimates of net primary production and yield of croplands, leading to improved quantification and understanding of the magnitude and geographic variation of CO$_2$ uptake by agroecosystems, i.e., carbon sequestration of croplands.

References

Baker, J.M., Griffis, T.J., 2005. Examining strategies to improve the carbon balance of corn/soybean agriculture using eddy covariance and mass balance techniques. Agric. For. Meteorol. 128 (3–4), 163–177.

Baker, J.M., Ochsner, T.E., Venterea, R.T., Griffis, T.J., 2007. Tillage and soil carbon sequestration – what do we really know? Agric. Ecosyst. Environ. 118 (1–4), 1–5.

Baldocchi, D., Falge, E., Gu, L.H., Olson, R., Hollinger, D., Running, S., Anthoni, P., Bernhofer, C., Davis, K., Evans, R., Fuentes, J., Goldstein, A., Katul, G., Law, B., Lee, X.H., Malhi, Y., Meyers, T., Munger, W., Oechel, W., U, K.T.P., Pilegaard, K., Schmid, H.P., Valentini, R., Verma, S., Vesala, T., Wilson, K., Wofsy, S., 2001. FLUXNET: A new tool to study the temporal and spatial variability of ecosystem-scale carbon dioxide, water vapor, and energy flux densities. Bull. m. Meteorol. Soc. 82 (11), 2415–2434.

Berry, J., Björkman, O., 1980. Photosynthetic response and adaptation to temperature in higher plants. Annu. Rev. Plant Phys. 31, 491–543.

Béziat, P., Ceschia, E., Dedieu, G., 2009. Carbon balance of a three crop succession over two cropland sites in South West France. Agric. For. Meteorol. 149 (10), 1628–1645.

Bhatti, A.U., Mulla, D.J., Frazier, B.E., 1991. Estimation of soil properties and wheat yields on complex eroded hills using geostatistics and Thematic Mapper images. Remote Sens. Environ. 37 (3), 181–191.

Boegh, E., Soegaard, H., Broge, N., Hasager, C.B., Jensen, N.O., Schelde, K., Thomsen, A., 2002. Airborne multispectral data for quantifying leaf area index, nitrogen concentration, and photosynthetic efficiency in agriculture. Remote Sens. Environ. 81 (2–3), 179–193.

Boles, S.H., Xiao, X.M., Liu, J.Y., Zhang, Q.Y., Munkhtuya, S., Chen, S.Q., Ojima, D., 2004. Land cover characterization of Temperate East Asia using multi-temporal VEGETATION sensor data. Remote Sens. Environ. 90 (4), 477–489.

Bradford, J.B., Hicke, J.A., Lauenroth, W.K., 2005. The relative importance of light-use efficiency modifications from environmental conditions and cultivation for estimation of large-scale net primary productivity. Remote Sens. Environ. 96 (2), 246–255.

Choudhury, B.J., 2001. Modeling radiation- and carbon-use efficiencies of maize, sorghum, and rice. Agric. For. Meteorol. 106 (4), 317–330.

Crafts-Brandner, S.J., Salvucci, M.E., 2002. Sensitivity of photosynthesis in a C_4 plant, maize, to heat stress. Plant Physiol. 129 (4), 1773–1780.

de Beurs, K.M., Henebry, G.M., 2004. Land surface phenology, climatic variation, and institutional change: analyzing agricultural land cover change in Kazakhstan. Remote Sens. Environ. 89 (4), 497–509.

Dobermann, A., Baker, J.M., Walters, D.T., 2006. Comment on "Carbon budget of mature no-till ecosystem in North Central Region of the United States". Agric. For. Meteorol. 136 (1), 83–84.

Dorigo, W.A., Zurita-Milla, R., de Wit, A.J.W., Brazile, J., Singh, R., Schaepman, M.E., 2007. A review on reflective remote sensing and data assimilation techniques for enhanced agroecosystem modeling. Int. J. Appl. Earth Obs. 9 (2), 165–193.

Ehleringer, J., Pearcy, R.W., 1983. Variation in quantum yield for CO2 uptake among C-3 and C-4 plants. Plant Physiol. 73 (3), 555–559.

Emerson, R., Lewis, C.M., 1941. Carbon dioxide exchange and the measurement of the quantum yield of photosynthesis. Am. J. Bot. 28 (9), 789–804.

Falge, E., Baldocchi, D., Olson, R., Anthoni, P., Aubinet, M., Bernhofer, C., Burba, G., Ceulemans, R., Clement, R., Dolman, H., Granier, A., Gross, P., Grunwald, T., Hollinger, D., Jensen, N.O., Katul, G., Keronen, P., Kowalski, A., Lai, C.T., Law, B.E., Meyers, T., Moncrieff, J., Moors, E., Munger, J.W., Pilegaard, K., Rannik, Ü., Rebmann, C., Suyker, A., Tenhunen, J., Tu, K., Verma, S., Vesala, T., Wilson, K., Wofsy, S., 2001a. Gap filling strategies for defensible annual sums of net ecosystem exchange. Agric. For. Meteorol. 107 (1), 43–69.

Falge, E., Baldocchi, D., Olson, R., Anthoni, P., Aubinet, M., Bernhofer, C., Burba, G., Ceulemans, R., Clement, R., Dolman, H., Granier, A., Gross, P., Grunwald, T., Hollinger, D., Jensen, N.O., Katul, G., Keronen, P., Kowalski, A., Lai, C.T., Law, B.E., Meyers, T., Moncrieff, J., Moors, E., Munger, J.W., Pilegaard, K., Rannik, Ü., Rebmann, C., Suyker, A., Tenhunen, J., Tu, K., Verma, S., Vesala, T., Wilson, K., Wofsy, S., 2001b. Gap filling strategies for long term energy flux data sets. Agric. For. Meteorol. 107 (1), 71–77.

Falge, E., Baldocchi, D., Tenhunen, J., Aubinet, M., Bakwin, P., Berbigier, P., Bernhofer, C., Burba, G., Clement, R., Davis, K.J., Elbers, J.A., Goldstein, A.H., Grelle, A., Granier, A., Guᵭmundsson, J., Hollinger, D., Kowalski, A.S., Katul, G., Law, B.E., Malhi, Y., Meyers, T., Monson, R.K., Munger, J.W., Oechel, W., U, K.T.P., Pilegaard, K., Rannik, Ü., Rebmann, C., Suyker, A., Valentini, R., Wilson, K., Wofsy, S., 2002a. Seasonality of ecosystem respiration and gross primary production as derived from FLUXNET measurements. Agric. For. Meteorol. 113 (1–4), 53–74.

Falge, E., Tenhunen, J., Baldocchi, D., Aubinet, M., Bakwin, P., Berbigier, P., Bernhofer, C., Bonnefond, J.M., Burba, G., Clement, R., Davis, K.J., Elbers, J.A., Falk, M., Goldstein, A.H., Grelle, A., Granier, A., Grunwald, T., Guᵭmundsson, J., Hollinger, D., Janssens, I.A., Keronen, P., Kowalski, A.S., Katul, G., Law, B.E., Malhi, Y., Meyers, T., Monson, R.K., Moors, E., Munger, J.W., Oechel, W., U, K.T.P., Pilegaard, K., Rannik, Ü., Rebmann, C., Suyker, A., Thorgeirsson, H., Tirone, G., Turnipseed, A., Wilson, K., Wofsy, S., 2002b. Phase and amplitude of ecosystem carbon release and uptake potentials as derived from FLUXNET measurements. Agric. For. Meteorol. 113 (1–4), 75–95.

Frank, A.B., Karn, J.F., 2003. Vegetation indices, CO2 flux, and biomass for Northern Plains Grasslands. J. Range Manage. 56 (4), 382–387.

Gao, Y., Duan, A.W., Qiu, X.Q., Sun, J.S., Zhang, J.P., Liu, H., Wang, H.Z., 2010. Distribution and use efficiency of photosynthetically active radiation in strip intercropping of maize and soybean. Agron. J. 102 (4), 1149–1157.

Gower, S.T., Kucharik, C.J., Norman, J.M., 1999. Direct and indirect estimation of leaf area index, f(APAR), and net primary production of terrestrial ecosystems. Remote Sens. Environ. 70 (1), 29–51.

Gwathmey, C.O., Tyler, D.D., Yin, X., 2010. Prospects for monitoring cotton crop maturity with Normalized Difference Vegetation Index. Agron. J. 102 (5), 1352–1360.

Hirasawa, T., Hsiao, T.C., 1999. Some characteristics of reduced leaf photosynthesis at midday in maize growing in the field. Field Crop. Res. 62 (1), 53–62.

Hollinger, S.E., Bernacchi, C.J., Meyers, T.P., 2005. Carbon budget of mature no-till ecosystem in North Central Region of the United States. Agric. For. Meteorol. 130 (1–2), 59–69.

Hollinger, S.E., Bernacchi, C.J., Meyers, T.P., 2006a. A reply to "Comment on 'Carbon budget of mature no-till ecosystem in North Central Region of the United States' by Dobermann et al." Agric. For. Meteorol. 136 (1), 85–87.

Hollinger, S.E., Bernacchi, C.J., Meyers, T.P., 2006b. Corrigendum to "Carbon budget of mature no-till ecosystem in North Central Region of the United States [Agric. For. Meteorol. 130 (2005) 59–69]". Agric. For. Meteorol. 136 (1), 88–89.

Huete, A., Didan, K., Miura, T., Rodriguez, E.P., Gao, X., Ferreira, L.G., 2002. Overview of the radiometric and biophysical performance of the MODIS vegetation indices. Remote Sens. Environ. 83 (1–2), 195–213.

Huete, A.R., Didan, K., Shimabukuro, Y.E., Ratana, P., Saleska, S.R., Hutyra, L.R., Yang, W.Z., Nemani, R.R., Myneni, R., 2006. Amazon rainforests green-up with sunlight in dry season. Geophys. Res. Lett. 33 (6), L06405.

Huete, A.R., Liu, H.Q., Batchily, K., vanLeeuwen, W., 1997. A comparison of vegetation indices over a global set of TM images for EOS-MO-DIS. Remote Sens. Environ. 59 (3), 440–451.

Jans, W.W.P., Jacobs, C.M.J., Kruijt, B., Elbers, J.A., Barendse, S., Moors, E.J., 2010. Carbon exchange of a maize (Zea mays L.) crop: influence of phenology. Agric. Ecosyst. Environ. 139 (3), 316–324.

Kim, S.H., Gitz, D.C., Sicherb, R.C., Baker, J.T., Timlin, D.J., Reddy, V.R., 2007. Temperature dependence of growth, development, and photosynthesis in maize under elevated CO2. Environ. Exp. Bot. 61 (3), 224–236.

Kiniry, J.R., Jones, C.A., Otoole, J.C., Blanchet, R., Cabelguenne, M., Spanel, D.A., 1989. Radiation-use efficiency in biomass accumulation prior to grain-filling for 5 grain-crop species. Field Crop. Res. 20 (1), 51–64.

Kubien, D.S., von Cammerer, S., Furbank, R.T., Sage, R.F., 2003. C-4 photosynthesis at low temperature. A study using transgenic plants with reduced amounts of Rubisco. Plant Physiol. 132 (3), 1577–1585.

Lei, H.M., Yang, D.W., 2010. Seasonal and interannual variations in carbon dioxide exchange over a cropland in the North China Plain. Global Change Biol. 16 (11), 2944–2957.

Li, Z.Q., Yu, G.R., Xiao, X.M., Li, Y.N., Zhao, X.Q., Ren, C.Y., Zhang, L.M., Fu, Y.L., 2007. Modeling gross primary production of alpine ecosystems in the Tibetan Plateau using MODIS images and climate data. Remote Sens. Environ. 107 (3), 510–519.

Lobell, D.B., Hicke, J.A., Asner, G.P., Field, C.B., Tucker, C.J., Los, S.O., 2002. Satellite estimates of productivity and light use efficiency in United States agriculture, 1982–98. Global Change Biol. 8 (8), 722–735.

Matsushita, B., Yang, W., Chen, J., Onda, Y., Qiu, G.Y., 2007. Sensitivity of the Enhanced Vegetation Index (EVI) and Normalized Difference Vegetation Index (NDVI) to topographic effects: a case study in high-density cypress forest. Sensors 7 (11), 2636–2651.

Mera, R.J., Niyogi, D., Buol, G.S., Wilkerson, G.G., Semazzi, F.H.M., 2006. Potential individual versus simultaneous climate change effects on soybean (C-3) and maize (C-4) crops: an agrotechnology model based study. Global Planet. Change 54 (1–2), 163–182.

Moors, E.J., Jacobs, C., Jans, W., Supit, I., Kutsch, W.L., Bernhofer, C., Beziat, P., Buchmann, N., Carrara, A., Ceschia, E., Elbers, J., Eugster, W., Kruijt, B., Loubet, B., Magliulo, E., Moureaux, C., Olioso, A., Saunders, M., Soegaard, H., 2010. Variability in carbon exchange of European croplands. Agric. Ecosyst. Environ. 139 (3), 325–335.

NASS, 2008. In: Board, A.S. (Ed.), Acreage. NASS, USDA, p. 40.

Osborne, C.P., Wythe, E.J., Ibrahim, D.G., Gilbert, M.E., Ripley, B.S., 2008. Low temperature effects on leaf physiology and survivorship in the C-3 and C-4 subspecies of Alloteropsis semialata. J. Exp. Bot. 59 (7), 1743–1754.

Ping, J.L., Dobermann, A., 2005. Processing of yield map data. Precis. Agric. 6 (2), 193–212.

Ping, J.L., Ferguson, R.B., Dobermann, A., 2008. Site-specific nitrogen and plant density management in irrigated maize. Agron. J. 100 (4), 1193–1204.

Prince, S.D., Goward, S.N., 1995. Global primary production: a remote sensing approach. J. Biogeogr. 22 (4–5), 815–835.

Raich, J.W., Rastetter, E.B., Melillo, J.M., Kicklighter, D.W., Steudler, P.A., Peterson, B.J., Grace, A.L., Moore, B., Vorosmarty, C.J., 1991. Potential net primary productivity in South America: application of a global model. Ecol. Appl. 1 (4), 399–429.

Reichstein, M., Falge, E., Baldocchi, D., Papale, D., Aubinet, M., Berbigier, P., Bernhofer, C., Buchmann, N., Gilmanov, T., Granier, A., Grunwald, T., Havránková, K., Ilvesniemi, H., Janous, D., Knohl, A., Laurila, T., Lohila, A., Loustau, D., Matteucci, G., Meyers, T., Miglietta, F., Ourcival, J.-M., Pumpanen, J., Rambal, S., Rotenberg, E., Sanz, M., Tenhunen, J., Seufert, G., Vaccari, F., Vesala, T., Yakir, D., Valentini, R., 2005. On the separation of net ecosystem exchange into assimilation and ecosystem respiration: review and improved algorithm. Global Change Biol. 11 (9), 1424–1439.

Ritchie, S.W., Hanway, J.J., Benson, G.O., 1992. How a corn plant develops. Iowa State Univ. Sci. Tech. Cooperative Ext. Services. Report No. 48. Iowa State University, Ames.

Rosati, A., Dejong, T.M., 2003. Estimating photosynthetic radiation use efficiency using incident light and photosynthesis of individual leaves. Ann. Bot. 91 (7), 869–877.

Ruimy, A., Jarvis, P.G., Baldocchi, D.D., Saugier, B., 1995. CO2 fluxes over plant canopies and solar radiation: a review. In: Begon, M., Fitter, A.H. (Eds.), Adv. Ecol. Res. Academic Press, pp. 1–68.

Running, S.W., Nemani, R.R., Heinsch, F.A., Zhao, M.S., Reeves, M., Hashimoto, H., 2004. A continuous satellite-derived measure of global terrestrial primary production. Bioscience 54 (6), 547–560.

Sage, R.F., Monson, R.K. (Eds.), 1999. C4 Plant Biology. Academic Press, San Diego, p. 596.

Sims, D.A., Rahman, A.F., Cordova, V.D., El-Masri, B.Z., Baldocchi, D.D., Bolstad, P.V., Flanagan, L.B., Goldstein, A.H., Hollinger, D.Y., Misson, L., Monson, R.K., Oechel, W.C., Schmid, H.P., Wofsy, S.C., Xu, L., 2008. A new model of gross primary productivity for North American ecosystems based solely on the enhanced vegetation index and land surface temperature from MODIS. Remote Sens. Environ. 112 (4), 1633–1646.

Sims, D.A., Rahman, A.F., Cordova, V.D., El-Masri, B.Z., Baldocchi, D.D., Flanagan, L.B., Goldstein, A.H., Hollinger, D.Y., Misson, L., Monson, R.K., Oechel, W.C., Schmid, H.P., Wofsy, S.C., Xu, L.K., 2006. On the use of MODIS EVI to assess gross primary productivity of North American ecosystems. J. Geophys. Res. G: Biogeosci. 111 (G4), G04015.

Sinclair, T.R., Muchow, R.C., 1999. Radiation use efficiency. Adv. Agron. Academic Press Inc., San Diego, pp. 215–265.

Singsaas, E.L., Ort, D.R., DeLucia, E.H., 2001. Variation in measured values of photosynthetic quantum yield in ecophysiological studies. Oecologia 128 (1), 15–23.

Stella, P., Lamaud, E., Brunet, Y., Bonnefond, J.M., Loustau, D., Irvine, M., 2009. Simultaneous measurements of CO2 and water exchanges over three agroecosystems in South-West France. Biogeosciences 6 (12), 2957–2971.

Sugiyama, T., 1973. Purification, molecular, and catalytic properties of pyruvate phosphate dikinase from maize leaf. Biochemistry 12 (15), 2862–2868.

Suyker, A.E., Verma, S.B., Burba, G.G., Arkebauer, T.J., 2005. Gross primary production and ecosystem respiration of irrigated maize and irrigated soybean during a growing season. Agric. For. Meteorol. 131 (3–4), 180–190.

Suyker, A.E., Verma, S.B., Burba, G.G., Arkebauer, T.J., Walters, D.T., Hubbard, K.G., 2004. Growing season carbon dioxide exchange in irrigated and rainfed maize. Agric. For. Meteorol. 124 (1–2), 1–13.

Tucker, C.J., 1979. Red and photographic infrared linear combinations for monitoring vegetation. Remote Sens. Environ. 8 (2), 127–150.

Tucker, C.J., Elgin, J.H., McMurtrey, J.E., Fan, C.J., 1979. Monitoring corn and soybean crop development with hand-held radiometer spectral data. Remote Sens. Environ. 8 (3), 237–248.

Verma, S.B., Dobermann, A., Cassman, K.G., Walters, D.T., Knops, J.M., Arkebauer, T.J., Suyker, A.E., Burba, G.G., Amos, B., Yang, H.S., Ginting, D., Hubbard, K.G., Gitelson, A.A., Walter-Shea, E.A., 2005. Annual carbon dioxide exchange in irrigated and rainfed maize-based agroecosystems. Agric. For. Meteorol. 131 (1–2), 77–96.

Vina, A., Gitelson, A.A., Rundquist, D.C., Keydan, G., Leavitt, B., Schepers, J., 2004. Remote sensing – monitoring maize (Zea mays L.) phenology with remote sensing. Agron. J. 96 (4), 1139–1147.

Wang, H.S., Jia, G.S., Fu, C.B., Feng, J.M., Zhao, T.B., Ma, Z.G., 2010a. Deriving maximal light use efficiency from coordinated flux measurements and satellite data for regional gross primary production modeling. Remote Sens. Environ. 114 (10), 2248–2258.

Wang, Z., Xiao, X., Yan, X., 2010b. Modeling gross primary production of maize cropland and degraded grassland in northeastern China. Agric. For. Meteorol. 150 (9), 1160–1167.

Wen, Q.K., Zhang, Z.X., Liu, S., Wang, X.A., Wang, C., 2010. Classification of grassland types by MODIS time-series images in Tibet, China. IEEE J. Sel. Top. Appl. Earth Observ. Remote Sens. 3 (3), 404–409.

Went, F.W., 1953. The effect of temperature on plant growth. Annu. Rev. Plant Phys. 4, 347–362.

Wofsy, S.C., Goulden, M.L., Munger, J.W., Fan, S.M., Bakwin, P.S., Daube, B.C., Bassow, S.L., Bazzaz, F.A., 1993. Net exchange of CO2 in a mid-latitude forest. Science 260 (5112), 1314–1317.

Wu, C., Munger, J.W., Niu, Z., Kuang, D., 2010a. Comparison of multiple models for estimating gross primary production using MODIS and eddy covariance data in Harvard Forest. Remote Sens. Environ. 114 (12), 2925–2939.

Wu, C.Y., Han, X.Z., Ni, J.S., Niu, Z., Huang, W.J., 2010b. Estimation of gross primary production in wheat from in situ measurements. Int. J. Appl. Earth Obs. 12 (3), 183–189.

Wu, C.Y., Niu, Z., Gao, S.A., 2010c. Gross primary production estimation from MODIS data with vegetation index and photosynthetically active radiation in maize. J. Geophys. Res. D: Atmos. 115, D12127.

Wu, J.B., Xiao, X.M., Guan, D.X., Shi, T.T., Jin, C.J., Han, S.J., 2009. Estimation of the gross primary production of an old-growth temperate mixed forest using eddy covariance and remote sensing. Int. J. Remote Sens. 30 (2), 463–479.

Wu, W.X., Wang, S.Q., Xiao, X.M., Yu, G.R., Fu, Y.L., Hao, Y.B., 2008. Modeling gross primary production of a temperate grassland ecosystem in Inner Mongolia, China, using MODIS imagery and climate data. Sci. China Ser. D-Earth Sci. 51 (10), 1501–1512.

Xiao, X.M., 2006. Light absorption by leaf chlorophyll and maximum light use efficiency. IEEE Trans. Geosci. Remote Sens. 44 (7), 1933–1935.

Xiao, X.M., Boles, S., Frolking, S., Li, C.S., Babu, J.Y., Salas, W., Moore, B., 2006. Mapping paddy rice agriculture in South and Southeast Asia using multi-temporal MODIS images. Remote Sens. Environ. 100 (1), 95–113.

Xiao, X.M., Braswell, B., Zhang, Q.Y., Boles, S., Frolking, S., Moore, B., 2003. Sensitivity of vegetation indices to atmospheric aerosols: continental-scale observations in Northern Asia. Remote Sens. Environ. 84 (3), 385–392.

Xiao, X.M., Hollinger, D., Aber, J., Goltz, M., Davidson, E.A., Zhang, Q.Y., Moore, B., 2004a. Satellite-based modeling of gross primary production in an evergreen needleleaf forest. Remote Sens. Environ. 89 (4), 519–534.

Xiao, X.M., Zhang, Q.Y., Braswell, B., Urbanski, S., Boles, S., Wofsy, S., Moore, B., Ojima, D., 2004b. Modeling gross primary production of temperate deciduous broadleaf forest using satellite images and climate data. Remote Sens. Environ. 91 (2), 256–270.

Xiao, X.M., Boles, S., Liu, J.Y., Zhuang, D.F., Frolking, S., Li, C.S., Salas, W., Moore, B., 2005a. Mapping paddy rice agriculture in southern China using multi-temporal MODIS images. Remote Sens. Environ. 95 (4), 480–492.

Xiao, X.M., Zhang, Q.Y., Hollinger, D., Aber, J., Moore, B., 2005b. Modeling gross primary production of an evergreen needleleaf forest using modis and climate data. Ecol. Appl. 15 (3), 954–969.

Xiao, X.M., Zhang, Q.Y., Saleska, S., Hutyra, L., De Camargo, P., Wofsy, S., Frolking, S., Boles, S., Keller, M., Moore, B., 2005c. Satellite-based modeling of gross primary production in a seasonally moist tropical evergreen forest. Remote Sens. Environ. 94 (1), 105–122.

Yan, H.M., Fu, Y.L., Xiao, X.M., Huang, H.Q., He, H.L., Ediger, L., 2009. Modeling gross primary productivity for winter wheat-maize double cropping system using MODIS time series and CO2 eddy flux tower data. Agric. Ecosyst. Environ. 129 (4), 391–400.

Yuan, W.P., Liu, S., Zhou, G.S., Zhou, G.Y., Tieszen, L.L., Baldocchi, D., Bernhofer, C., Gholz, H., Goldstein, A.H., Goulden, M.L., Hollinger, D.Y., Hu, Y., Law, B.E., Stoy, P.C., Vesala, T., Wofsy, S.C., Collaborators, A., 2007. Deriving a light use efficiency model from eddy covariance flux data for predicting daily gross primary production across biomes. Agric. For. Meteorol. 143 (3–4), 189–207.

Yuan, W.P., Liu, S.G., Yu, G.R., Bonnefond, J.M., Chen, J.Q., Davis, K., Desai, A.R., Goldstein, A.H., Gianelle, D., Rossi, F., Suyker, A.E., Verma, S.B., 2010. Global estimates of evapotranspiration and gross primary production based on MODIS and global meteorology data. Remote Sens. Environ. 114 (7), 1416–1431.

Zhang, Q.Y., Xiao, X.M., Braswell, B., Linder, E., Baret, F., Moore, B., 2005. Estimating light absorption by chlorophyll, leaf and canopy in a deciduous broadleaf forest using MODIS data and a radiative transfer model. Remote Sens. Environ. 99 (3), 357–371.

Zhang, Q.Y., Xiao, X.M., Braswell, B., Linder, E., Ollinger, S., Smith, M.L., Jenkins, J.P., Baret, F., Richardson, A.D., Moore, B., Minocha, R., 2006a. Characterization of seasonal variation of forest canopy in a temperate deciduous broadleaf forest, using daily MODIS data. Remote Sens. Environ. 105 (3), 189–203.

Zhang, X.Y., Friedl, M.A., Schaaf, C.B., 2006b. Global vegetation phenology from moderate resolution imaging spectroradiometer (MODIS): evaluation of global patterns and comparison with in situ measurements. J. Geophys. Res. G: Biogeosci. 111 (G4), G04017.

Zhang, X.Y., Friedl, M.A., Schaaf, C.B., Strahler, A.H., Hodges, J.C.F., Gao, F., Reed, B.C., Huete, A., 2003. Monitoring vegetation phenology using MODIS. Remote Sens. Environ. 84 (3), 471–475.